博士論文（要約）

Studies on ionization and coherent rotational motion of linear triatomic molecules induced by intense laser pulses

(高強度レーザー光により誘起される直線三原子分子の

イオン化とコヒーレント回転運動の研究)

園田 浩太郎

Acknowledgements

I would like to sincerely thank Dr. Hirokazu Hasegawa, my advisor, for giving me the opportunity to work in his group. I appreciate his support and encouragement.

I would also like to thank Dr. Kaoru Yamanouchi and Dr. Atsushi Iwasaki for their support, fruitful discussions and valuable suggestions.

Summary of notation

X, Y, Z : space-fixed axes

x, y, z : molecule-fixed axes

φ, θ, χ : Euler angles

$\boldsymbol{J}$: total angular momentum

$\boldsymbol{L}$: electronic orbital angular momentum

$\boldsymbol{S}$: electronic spin angular momentum

$\boldsymbol{N}$: total angular momentum excluding electron spin, i.e., $\boldsymbol{N} = \boldsymbol{J} - \boldsymbol{S}$

M : projection of $\boldsymbol{J}$ onto the Z axis in the space-fixed frame.

Λ : projection of $\boldsymbol{L}$ onto the internuclear axis

Σ : projection of $\boldsymbol{S}$ onto the internuclear axis

Ω : projection of $\boldsymbol{J}$ onto the internuclear axis

B : rotational constant in units of Joule

$\tilde{B}$: rotational constant in units of cm^{-1}

$\tilde{D}$: centrifugal distortion constant in units of cm^{-1}

A : spin-orbit coupling constant in units of cm^{-1}

γ : spin-rotation coupling constant in units of cm^{-1}

$\tilde{F}(J)$: rotational energy in units of cm^{-1}

$E_{\mathrm{rot}}(J)$: rotational energy in units of Joule

h : Plank's constant

c : velocity of light in vacuum

m_{e} : mass of an electron

e : absolute value of the electron charge

k_{B} : Boltzmann constant

μ : dipole moment

α_{pq}, α_{PQ} : components of polarizability tensor ($p,q = x, y, z$; $P,Q = X, Y, Z$)

β_{pqr} : hyperpolarizability ($p,q,r = x, y, z$)

H : Hamiltonian

$D^{j}_{m,m'}(\varphi, \theta, \chi)$: elements of $(2j+1)\times(2j+1)$ Wigner rotational matrix

$\boldsymbol{E}(t)$: electric field

I : focal intensity of laser

λ : wavelength

ω : angular frequency of optical fields

T_{rot} : rotational temperature

τ_{rot} : rotational period

t : time

γ_{K} : Keldysh parameter

I_p : ionization potential

W : ionization probability

Γ : ionization rate

U_p : pondermotive energy

Z_{rot} : rotational partition function

Table of contents

Chapter 1

Introduction

1.1 Ultrafast processes induced by intense laser pulses

In order to observe ultrafast dynamical processes of atoms and molecules in real time, various technologies for generating ultrashort laser pulses have been developed [1-5] since the first laser was built by Maiman [6]. Nowadays, table-top femtosecond (10^{-15} s) laser systems are commercially available. Such ultrashort laser pulses are suitable for following rotational [7] and vibrational [8] motions of molecules in real time because of their high temporal resolution. Recent development in laser technology can allow us to use even shorter laser pulses whose pulse width is several hundreds or tens of attoseconds (10^{-18} s) [9-11], which can follow valence electron motion in real time [12, 13].

Aside from the generation of the ultrashort laser pulses, technological advances in increasing laser power are also remarkable [5, 14]. The peak power of the ultrashort laser pulses was limited because high-power short laser pulses cause damage to an active medium of an amplifier. However, a novel method of amplification, called chirped-pulse amplification (CPA) [15], broke the limitation and brought a breakthrough [16].

These developments in laser technology have changed quality of light sources dramatically and have opened up a new research field called strong-field physics (see refs. [17-23] for reviews). When a high-power laser pulse with a duration of several femtoseconds is focused onto a small area by an optical lens, a focal intensity of 10^{12} - 10^{16} W/cm^2 can be easily achieved because much energy is concentrated into a small volume in a very short period of time. The corresponding strength of an electric field is on the order of 10^7 - 10^9 V/cm, which is comparable to the strength of a Coulomb field in atomic and molecular systems.

One of the most common phenomena induced by the intense laser pulses is ionization [24-27]. When atoms and molecules are irradiated with the intense laser pulses whose photon energy is much lower than ionization potential, they can be ionized by absorbing several photons. This phenomenon, known as multiphoton ionization, was observed in 1963 [28] and can be interpreted within a frame of the lowest-order perturbation theory (LOPT) [29]. According to the LOPT, the *n*-photon ionization rate is proportional to I^n, where I is the laser intensity.

A crucial breakthrough has been brought by the observation of a new ionization process, called above-threshold ionization (ATI) [30]. It has been found that an electron ejected from Xe via an ionization process can absorb additional photons in excess of the minimum number required for ionizing atoms [30]. Several peaks separated by the photon energy appear in a photoelectron spectrum. This characteristic structure of the photoelectron spectrum is called the ATI structure. Interestingly, yields of the ATI photoelectrons that have high kinetic energy do not obey the LOPT when the laser intensity is sufficiently high [31]. The breakdown of the LOPT clearly shows that the intense laser pulses cannot be regarded as a perturbation anymore. The required intensity to induce such non-perturbative effects is higher than 5×10^{12} W/cm^2 [21].

As the laser intensity increases, another ionization process, called tunneling ionization [32], becomes dominant. A CO_2 laser, whose wavelength is 10.55 μm or 9.55 μm, was used in the first experiment of the tunneling ionization [33] because this ionization process is effectively induced when the wavelength of the laser pulse is relatively long. In recent studies on the tunneling ionization and other strong-field phenomena, a titanium-doped sapphire laser with a central wavelength of 800 nm [34] has been commonly used. In this ionization process, the laser field behaves as an electric field rather than a photon. As shown in Fig. 1.1, a binding potential of electrons in an atomic system is distorted by the laser field when the laser intensity is sufficiently high. The significant distortion of the binding potential occurs with a period of 1.33 fs, which corresponds to a half of the optical period of Ti:Sapphire laser pulses. A potential barrier is formed because of the combination of the Coulomb potential and laser field. Electrons can tunnel through this barrier.

As described above, there are two ionization mechanisms: multiphoton ionization and tunneling ionization. The Keldysh parameter γ_K is often used to estimate which

mechanism is dominant. This parameter is defined as

$$\gamma_{\mathrm{K}}=\sqrt{\frac{I_P}{2U_p}}, \tag{1.1}$$

where I_{P} is the ionization potential and U_{p} is the ponderomotive energy [32]. The pondermotive energy, which is also known as the cycle-averaged kinetic energy of a quivering electron in a laser field, is given by

$$U_{\mathrm{p}}=\frac{e^2E^2}{4m_{\mathrm{e}}\omega^2}, \tag{1.2}$$

where e is the absolute value of the electron charge, E is the electric field strength, m_{e} is the mass of an electron, and ω is the angular frequency of the laser field. The tunneling ionization is a dominant process when γ_{K} is much lower than 1, which means that a low frequency and high intensity are required for this ionization process [32]. These conditions allow electrons to have enough time to go through the potential barrier. Although Keldysh parameter is a good indicator for distinguishing the multiphoton ionization and tunneling ionization, it should be noted that both mechanisms can contribute to the ionization process at the same time under some conditions. In fact, the contribution of the tunneling ionization is still present even when $\gamma_{\mathrm{K}}>1$ [27]. Another empirical indicator for distinguishing the two ionization processes is ATI structures in photoelectron spectra [18]. As the laser intensity increases, the ATI structures in the spectra vanish. The change of spectral structures can be regarded as a sign of transition from the multiphoton ionization to the tunneling ionization [18, 35].

In order to have a better understanding of the tunneling ionization process in atomic systems, various analytic formulae of ionization rate have been proposed [32, 36-41]. The tunneling ionization rate of hydrogen atoms in the ground state was derived by Landau [41]. The derived formula shows an exponential dependence on a field strength. Basically, the tunneling ionization rate of any atoms is governed by the exponential factor, $\exp(-2\kappa^3/(3E))$, with $\kappa = (2I_{\mathrm{P}})^{1/2}$ [25]. A typical ionization rate of hydrogen atoms is shown by a green shade in Fig. 1.1. As can be seen, the ionization rate is increased only when the amplitude of the laser field is large. In other words, atoms are ionized every 1.33 fs if the wavelength of the laser pulse is 800 nm. The tunneling ionization occurs in a very short time (~ 700 as). Therefore, the tunneling ionization itself is an ultrafast phenomenon.

The proposed formulae of the ionization rate have been tested by comparing calculated ion yields with measured ones [42-44]. Since the intensity of laser pulses changes with time, it is necessary to obtain ionization probability by integrating the ionization rate over *t*. According to a rate equation, the ionization probability *W* is given by

$$W = 1 - \exp\left(-\int_{-\infty}^{\infty} \Gamma_{\mathrm{TI}}(t)dt\right), \tag{1.3}$$

where $\Gamma_{\mathrm{TI}}(t)$ is the tunneling ionization rate. One of the most commonly used formulae for calculating the ionization rate was proposed by Ammosov, Delone, and Krainov (ADK) in 1986 [40]. It has been shown that the dependence of atomic ion yields on the laser intensity is well reproduced by the ADK formula [42].

Electrons ejected via the tunneling ionization process can trigger other interesting phenomena, such as high-order harmonic generation (HHG) [45-47] and non-sequential double ionization (NSDI) [48, 49]. These novel phenomena are well explained by the three-step model [47]. The first step of this model is an ejection of an electron via the tunneling ionization process. In the second step, the ejected electron is accelerated by the laser field and returns back towards the ion core with high kinetic energy because the laser field oscillates with time. Finally, the accelerated electron collides with the ion core. The non-sequential double ionization is induced if the colliding electron has sufficient energy to ionize the singly-charged ion. It has been found that the contribution of the non-sequential double ionization is large at low intensity region for He [48-50] and Ne [50]. As the laser intensity increases, sequential double ionization (SDI) plays an important role. In the sequential double ionization, singly-charged ions generated by intense femtosecond laser pulses are further ionized in the laser fields. The dependence of a doubly-charged ion yield on the laser intensity is well reproduced by calculation based on the ADK formula when the laser intensity is sufficiently high, which assures that the sequential double ionization is a responsible process. If the colliding electron is captured in the ionic core, the excess energy is released as high-energy radiation, known as high-order harmonics.

In contrast to atoms, strong-field ionization of molecules is still unclear because complexity of molecules leads to rich dynamics. In fact, the ionization of molecules is often followed by dissociation. If multiply-charged molecular ions are produced by the

intense laser pulses, most of them dissociate into fragment ions immediately because of a Coulomb repulsive force between positively-charged atomic ions. This phenomenon is known as Coulomb explosion. The kinetic energies of fragments produced by the Coulomb explosion have information on a molecular structure just before the fragmentation. If the multiple ionization of diatomic molecules occurs at an equilibrium internuclear distance, Coulomb-exploded fragments have large kinetic energy. In contrast, the kinetic energy of the fragments is smaller if the multiple ionization occurs at a longer internuclear distance. For polyatomic molecules, the directions of ejected fragments are also important because they reflect a bond angle just before the Coulomb explosion. In fact, detailed analyses of released kinetic energies and directions of Coulomb-exploded fragments have revealed that the structures of triatomic molecules are strongly deformed in the intense laser fields [51-70]. The concept of light-dressed potential energy surfaces is helpful to understand the ultrafast structural deformation [71]. For polyatomic molecules containing hydrogen atoms, ultrafast dynamics of hydrogen atoms or protons,

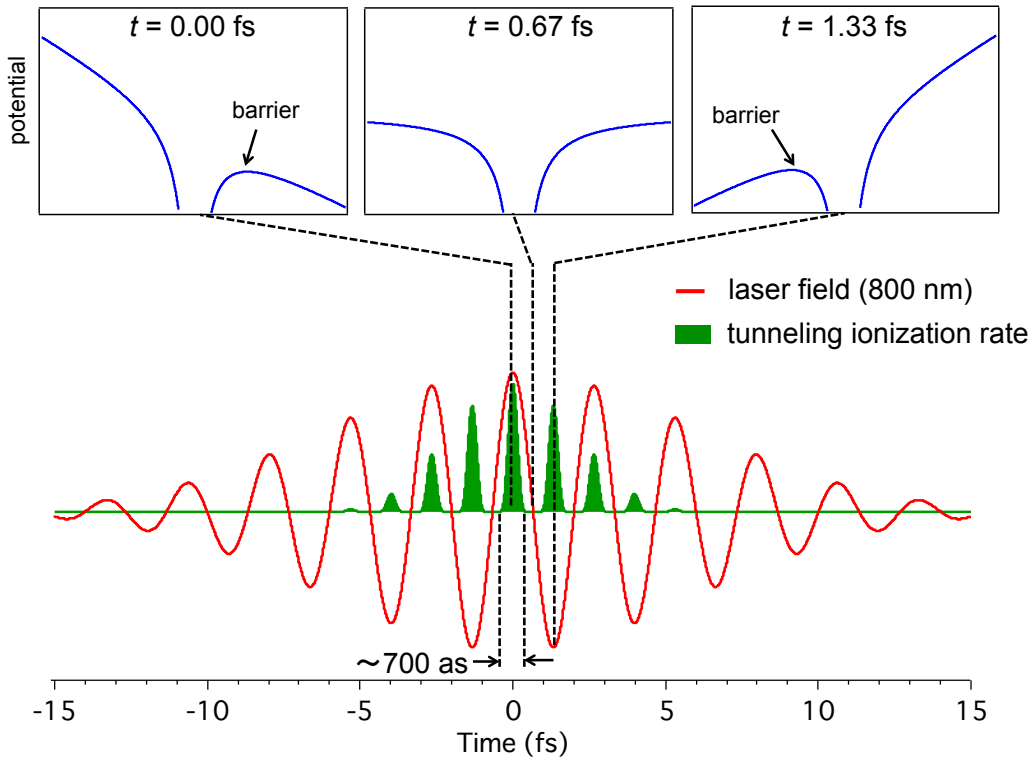

Figure 1.1: Tunneling ionization of a hydrogen atom. Distorted potentials of the atom in an intense laser pulse at 0.0, 0.67, and 1.33 fs are shown by blue curves in top panels. The ionization rate is calculated using the formula given by Landau [41]. The 10-fs laser pulse with an intensity of 2.0×10^{14} W/cm^2 is assumed.

called hydrogen migration, has been well investigated [72].

In addition to the dissociative ionization of molecules, ionization processes associated with a generation of stable singly-charged molecular ions have been also investigated to reveal differences between molecules and atoms in the strong-field ionization [73-77]. As mentioned before, the tunneling ionization rate is mainly governed by the exponential factor that includes ionization potential and laser intensity [25]. It is, therefore, expected that ion yields of atoms and molecules are the same at a specific laser intensity if they have similar ionization potentials. In order to verify this prediction, the ion yields of various atoms and molecules have been measured as a function of laser intensity [73-77]. The ion yields of N_2 (I_p = 15.58 eV) and Ar (I_p = 15.76 eV) show the same dependence on the laser intensity [74]. However, the ion yield of O_2 (I_p = 12.03 eV) is lower than that of Xe (I_p = 12.13 eV) [74], which contradicts with the prediction. Several theoretical models have been proposed to explain the difference between the yields of atomic and molecular ions [78-81]. The molecular Ammosov-Delone-Krainov (MO-ADK) theory [81] is one of the most widely adopted theories that can explain this discrepancy. According to this theory, the difference between the O_2^+ and Xe^+ yields is due to the dependence of the ion yield on the angle between the molecular axis and the polarization direction of the laser pulse. The MO-ADK theory provides an analytical formula for calculating tunneling ionization rate of molecules [81]:

$$\Gamma_{\mathrm{TI}}=\sum_{m'}\frac{|B_{m'}|^2}{2^{|m'|}}\frac{1}{|m'|!}\frac{1}{\kappa^{2Z_C/\kappa-1}}\left(\frac{2\kappa^3}{F}\right)^{2Z_C/\kappa-|m'|-1}\exp\left(-\frac{2\kappa^3}{3F}\right), \tag{1.4}$$

where

$$|B_{m'}|^2=\left[\sum_l C_l D^l_{m'm}(\mathbf{R})Q_{lm'}\right]^2 \tag{1.5}$$

and

$$Q_{lm}=(-1)^m\sqrt{\frac{(2l+1)(l+|m|)!}{2(l-|m|)!}}. \tag{1.6}$$

Here, C_l is the structural parameter, $D^l_{m'm}(\mathbf{R})$ is the Wigner D matrix element, and $\mathbf{R}$ represents Euler angles. In Eq. (1.4), $|B_m|^2$ is responsible for the angular dependence of the ionization rate, which reflects the shape of the highest-occupied molecular orbital

(HOMO). The ionization rate of the MO-ADK theory includes the exponential factor, $\exp(-2\kappa^3/(3E))$, as in the ADK theory. Low ionization potential and high laser intensity are required for increasing the tunneling ionization rate of molecules because the magnitude of this rate is mainly governed by this exponential factor. It should be noted that electrons can be ejected from lower-lying orbitals [82-89]. However, the contribution of such orbitals to the tunneling ionization is relatively small because they have high ionization potentials compared to the HOMO.

One of the most promising techniques for investigating the strong-field ionization of molecules is nonadiabatic molecular alignment [90-92]. Various rotational eigenstates are coherently populated via a series of rotational Raman excitations by linearly-polarized intense femtosecond laser pulses, which results in a creation of a rotational wave packet. Molecular axis distribution localizes periodically along the polarization direction of the laser pulses. This technique enables us to fix molecular axes in space under a field-free condition because the rotational wave packet evolves with time after the laser field vanishes. After the first experimental demonstration of this technique [7], the dependence of ion yields on the angle between the molecular axis and the polarization direction of laser pulses was investigated for linear molecules and compared with calculations based on the MO-ADK theory [93]. For N_2 and O_2, it has been verified that the angular dependence of ion yields reflects the shape of the HOMO [93].

The strong-field ionization of molecules is important amongst the various phenomena induced by intense femtosecond laser pulses because it can be the first step of other phenomena. Moreover, the strong-field ionization, which is often followed by dissociation, can be used as probes of chemical reactions [94, 95], wave-packet dynamics [7, 95-101], molecular orbitals [93, 102], molecular structure [103, 104], and electron correlation [105]. Unveiling the strong-field ionization process of molecules is desired to understand various strong-field phenomena following the ionization and broaden the possibility of application for probing molecular properties and dynamics. Most studies on the ionization process, however, have focused on dissociation processes following the ionization. Ionization processes associated with production of stable molecular ions have not been investigated intensively even though these ions can be produced as intermediate species of various strong-field phenomena. It is necessary to prepare axis-controlled molecules to study the strong-field ionization of molecules because the ionization

probability depends on the angle between the molecular axis and polarization direction of the laser pulses. In addition to fixing the molecular axis in space, distinguishing the head and tail of a polar molecule, i.e., control of molecular orientation, is also required to obtain deep insight into the strong-field ionization of molecules. However, techniques for controlling molecular orientation are still immature compared to those for controlling molecular alignment. Vibrational- and rotational-state distributions of molecular ions produced by intense femtosecond laser pulses should be also revealed to have a deep understanding of the strong-field ionization because they reflect how the molecules interact with the laser pulses and how molecular ions are generated. Although there are a few experimental studies on the vibrational-state distribution of H_2^+ [106, 107], rotational-state distribution of other molecular ions in the electronic ground state has not been investigated.

1.2 Thesis Outline

The primary goal of this thesis is to unveil the ultrafast strong-field ionization of molecules, especially processes associated with the production of molecular ions. This thesis is structured as follows.

Chapter 1 serves as an introduction to ultrafast strong-field phenomena, especially the strong-field ionization. The first aim of this chapter is to provide a research background, which is required to understand works in this thesis. The second aim of this chapter is to establish and emphasize the importance of the strong-field ionization.

Chapter 2 describes theoretical fundamentals for controlling molecular axis distribution, i.e., molecular alignment and orientation. In order to have a deep understanding of the strong-field ionization, control of molecular axis distribution is a promising technique because this ionization process depends on the angle between the polarization direction of the laser pulses and molecular axis.

In Chapter 3, multiple-ionization processes of axis-controlled OCS is investigated using a pump-probe method, in which the pump pulse prepares aligned OCS molecules based on the technique described in Chapter 2 and the probe pulse ionizes molecules. It is shown that the yields of OCS^{2+} and OCS^{3+} are very sensitive to a change of molecular axis distribution. The dependences of the OCS^{2+} and OCS^{3+} yields on the angle between the molecular axis and polarization direction of the ionizing laser pulse are obtained. These angular dependences are expected to be useful for understanding succeeding dissociation processes.

Chapter 4 is devoted to the enhancement and control of molecular orientation, which is a desired technique for understanding the ionization process of molecules deeply. An intense laser pulse and two-color intense laser pulses are used to orient molecules. The dependence of the orientation dynamics on delay between the two laser pulses is investigated for the first time.

In Chapter 5, spectroscopic studies on N_2O^+ produced by intense femtosecond laser pulses are presented. In contrast to Chapter 3, the ionization process is investigated in terms of vibrational- and rotational-state distributions. Differences between ionization processes by perturbative and non-perturbative lights are discussed based on obtained vibrational- and rotational-state distributions.

Chapter 6 summarizes the whole chapters in this thesis.

Chapter2

Rotational Motion of Molecules

In this thesis, ionization and coherent rotational motion of carbonyl sulfide (OCS) and nitrous oxide (N_2O) are investigated. This chapter provides theoretical fundamentals that are necessary for understanding the rotational motion of these molecules and cations. In the former part of this chapter, formulae of rotational energy are presented for OCS ($\tilde{X}\ ^1\Sigma^+$), N_2O ($\tilde{X}\ ^1\Sigma^+$), and N_2O^+ ($\tilde{X}\ ^2\Pi$ and $\tilde{A}\ ^2\Sigma^+$). The latter part of this chapter includes theoretical details about coherent rotational dynamics of these molecules and cations.

2.1 Rotational energy levels of molecules and ions

2.1.1 OCS ($\tilde{X}\ ^1\Sigma^+$) and N_2O ($\tilde{X}\ ^1\Sigma^+$)

The electronic configurations of OCS and N_2O are expressed as

$$[(1\sigma)^2\ (2\sigma)^2\ (3\sigma)^2\ (4\sigma)^2\ (5\sigma)^2(1\pi)^4]\ (6\sigma)^2\ (7\sigma)^2\ (8\sigma)^2\ (9\sigma)^2\ (2\pi)^4\ (3\pi)^4$$

and

$$[(1\sigma)^2\ (2\sigma)^2\ (3\sigma)^2]\ (4\sigma)^2\ (5\sigma)^2\ (6\sigma)^2\ (1\pi)^2\ (7\sigma)^2\ (2\pi)^4,$$

respectively. Here, orbitals in the square brackets are core orbitals. For these linear molecules, the molecular term symbols of the electronic ground states are represented by $\tilde{X}\ ^1\Sigma^+$. In a $^1\Sigma^+$ state, rotational energy $E_{rot}(J)$ is expressed by a simple form that depends only on the total angular momentum quantum number, J:

$$E_{rot}(J) = BJ(J+1), \tag{2.1}$$

where B is the rotational constant in units of Joule. This formula can be expressed in terms of cm^{-1} as

$$\tilde{F}(J) = E_{rot}(J)/(100hc) = \tilde{B}J(J+1), \tag{2.2}$$

where $\tilde{B}$ is the rotational constant in units of cm^{-1}. The rotational constants of OCS and

N_2O are reported to be 0.202856753 cm^{-1} and 0.419011034 cm^{-1}, respectively [108]. Equations (2.1) and (2.2) are valid only when a molecule can be regarded as a rigid rotor.

The rotational energies of OCS and N_2O are calculated using Eq. (2.2) and shown in Fig. 2.1. In this figure, the signs, + and −, represent total parity, which reflects how the sign of a molecular wave function changes by applying a space-fixed inversion operator. The positive sign, +, means that the inversion operator leaves the total molecular wave function unchanged. On the other hand, the negative sign, −, means the sign of the wave function is changed by the inversion operator. The total parity alternates with *J* for OCS and N_2O in the $\tilde{X}\ ^1\Sigma^+$ state.

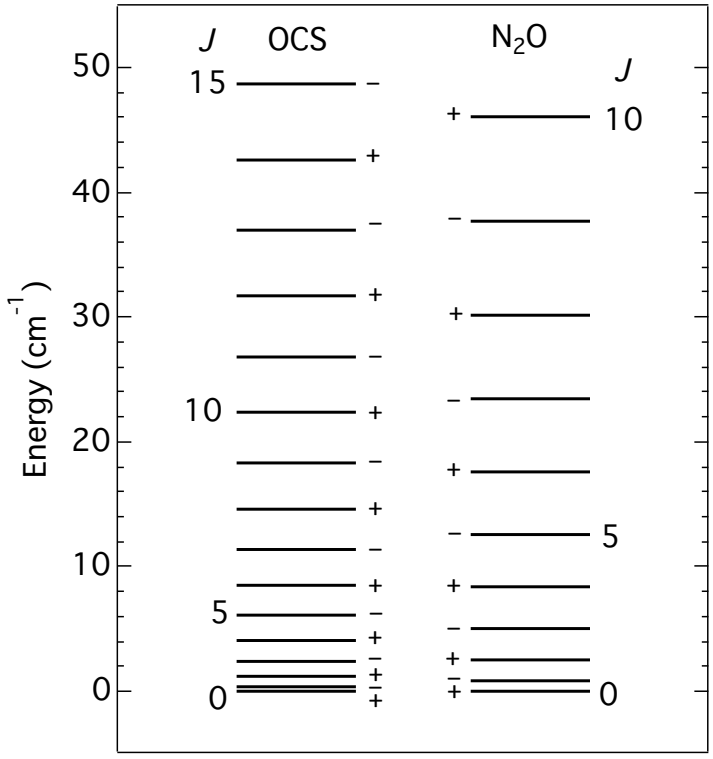

Figure 2.1: Rotational energy levels of OCS and N_2O in the electronic ground state. Both molecules are assumed to be rigid rotors. Total parity of each level is denoted by + and −.

2.1.2 N_2O^+ ($\tilde{X}\ ^2\Pi$)

Nitrous oxide cation (N_2O^+) in the electronic ground state is a linear molecular ion that has an unpaired electron. The electron configuration is expressed as [109]

$$[(1\sigma)^2\ (2\sigma)^2\ (3\sigma)^2]\ (4\sigma)^2\ (5\sigma)^2\ (6\sigma)^2\ (1\pi)^2\ (7\sigma)^2\ (2\pi)^3.$$

The molecular term symbol of the electronic ground state is represented by $\tilde{X}\ ^2\Pi$. This electronic state is well described by Hund's coupling case (a) [110]. In this coupling scheme, good quantum numbers are J, Ω, Λ, S, and Σ.

In a $^2\Pi$ state, the possible values of $|\Omega|$ are 0.5 and 1.5 because of $|\Lambda| = 1$ and $|\Sigma| = 0.5$. The two electronic states associated with $|\Omega| = 0.5$ and 1.5 are separated by 133 cm^{-1} because of the spin-orbit interaction [111]. The two split states, $\tilde{X}\ ^2\Pi_{3/2}$ and $\tilde{X}\ ^2\Pi_{1/2}$, are called the F_1 component and F_2 component, respectively.

Compared to rovibrational energy levels of linear triatomic molecules in $^1\Sigma^+$ states, those of linear triatomic molecules in $^2\Pi$ states can be quite complex [112]. In degenerate electronic states (e.g., Π, Δ, and other electronic states, except for Σ), an orbital angular momentum of electrons lies along the molecular axis. An angular momentum arisen from degenerate bending vibrations is coupled with this electronic angular momentum. As a result, a vibronic angular momentum is created. The vibrational angular momentum has two possible orientations along the internuclear axis with the magnitude of $\pm l$, where l is the quantum number of the vibrational angular momentum along the molecular axis. Hence, the vibronic angular momentum is $\hbar K$, where $K=|\pm\Lambda\pm l|$. Because of the vibronic angular momentum, the rotational energy levels depend on J and K as shown below [112, 113]:

$$\tilde{F}(J,K) = \tilde{B}x - \tilde{D}\left\{x^2 + \left(J+\frac{1}{2}\right)^2\right\} \pm \frac{1}{2}\sqrt{4\left(\tilde{B}^* - \frac{1}{2}\gamma\right)^2 + \left(A - 2\tilde{B}^*K\right)^2}, \qquad (2.3)$$

where $\tilde{D}$ is the centrifugal distortion constant, γ is the spin-rotation coupling constant, A is the spin-orbit coupling constant, $x = (J + 1/2)^2 - K^2$, and $\tilde{B}^* = \tilde{B} - 2\tilde{D}x$. The molecular constants of N_2O^+ in the $\tilde{X}\ ^2\Pi$ (000) state are determined as $\tilde{B}$ = 0.41026 cm^{-1}, $\tilde{D}$ = 1.74×10^{-7} cm^{-1}, A = −132.35508 cm^{-1}, and γ = −0.014237763 cm^{-1} [110, 113]. Here, three integers in parentheses represent vibrational quantum numbers of symmetric stretching, bending, and anti-symmetric stretching modes in order. The signs, − and +, before the square root are associated with the F_1 component and the F_2 component,

respectively. The effect of the Λ-doubling can be considered by adding the correction term to the Eq. (2.3) [114]. A schematic diagram of rotational levels is shown in Fig. 2.2. Because J cannot be lower than $|\Omega|$, the lowest J of the F_1 and F_2 components are 1.5 and 0.5, respectively.

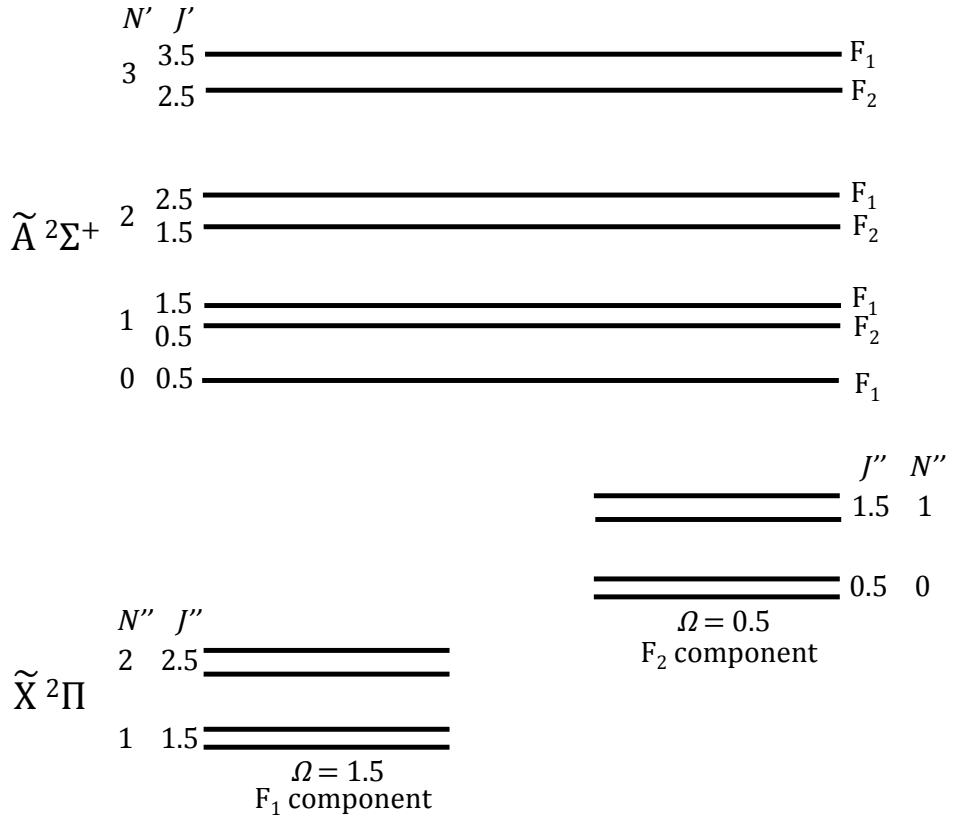

Figure 2.2: A schematic diagram for the energy levels of the $\tilde{X}\ ^2\Pi_{3/2,\ 1/2}$ and $\tilde{A}\ ^2\Sigma^+$ states of N_2O^+. The spin-rotation splitting in the $\tilde{A}\ ^2\Sigma^+$ state and the Λ-doubling in the $\tilde{X}\ ^2\Pi$ state are exaggerated.

2.1.3 N_2O^+ ($\tilde{A}\ ^2\Sigma^+$)

The first electronic excited state of N_2O^+ is the $\tilde{A}\ ^2\Sigma^+$ state. This state is well described by Hund's coupling case (b). Good quantum numbers for this coupling scheme are Λ, N, S, and J. Rotational energy is calculated by the following equations [113, 115]:

$$\tilde{F}(N) = \tilde{B}N(N+1) - \tilde{D}N^2(N+1)^2 + \frac{1}{2}\gamma N \quad (F_1 \text{ component}) \tag{2.4}$$

$$\tilde{F}(N) = \tilde{B}N(N+1) - \tilde{D}N^2(N+1)^2 - \frac{1}{2}\gamma(N+1) \quad (F_2 \text{ component}) \tag{2.5}$$

Here, F_1 and F_2 denote levels with $J = N + 1/2$ and $J = N - 1/2$, respectively. A schematic diagram of rotational levels is represented in Fig. 2.2. The molecular constants of N_2O^+ in the $\tilde{A}\ ^2\Sigma^+$ (200) state are reported to be $\tilde{B}$ = 0.42893 cm^{-1}, $\tilde{D}$ = 1.6 × 10^{-7} cm^{-1}, and γ = 0.0013 cm^{-1} [110].

2.2 Molecular alignment and orientation

2.2.1 Theoretical fundamentals on molecular alignment

When a nonresonant femtosecond laser pulse is strong enough to induce a dipole moment in a molecule, molecular alignment is achieved via the interaction between the induced dipole moment and laser pulse [116]. The interaction potential is given by

$$V_{\mathrm{p}}\big(E(t)\big) = -\frac{1}{2}{}^{t}\boldsymbol{E}(t)\boldsymbol{\alpha}\boldsymbol{E}(t), \tag{2.6}$$

where $\boldsymbol{\alpha}$ is the polarizability tensor and $\boldsymbol{E}(t)$ is the electric field vector. If the electric field of the laser pulse oscillates along the Z axis in the space-fixed frame, the interaction potential is reduced to

$$V_{\mathrm{p}}\big(E(t)\big) = -\frac{1}{2}\begin{pmatrix}0 & 0 & E(t)\end{pmatrix}\begin{pmatrix}\alpha_{XX} & \alpha_{XY} & \alpha_{XZ}\\ \alpha_{XY} & \alpha_{YY} & \alpha_{YZ}\\ \alpha_{XZ} & \alpha_{YZ} & \alpha_{ZZ}\end{pmatrix}\begin{pmatrix}0\\0\\E(t)\end{pmatrix} = -\frac{1}{2}\alpha_{ZZ}[E(t)]^2. \tag{2.7}$$

Here, α_{PQ} (P, Q = X, Y, Z) is the tensor component of the polarizability in the space-fixed frame. The electric field of the linearly-polarized laser pulse is expressed by

$$E(t) = \varepsilon(t)\cos\omega t, \tag{2.8}$$

where $\varepsilon(t)$ is the envelope function of the laser pulse and ω is the angular frequency of the laser field. Equation (2.7) is inconvenient because the value of α_{ZZ} changes if the molecule rotates. Therefore, it would be more reasonable to express α_{ZZ} by tensor components in the molecule-fixed frame, α_{pq} (p, q = x, y, z). Such transformation can be carried out by the direction cosine matrix $\boldsymbol{\Phi}_{\mathrm{d}}$ as shown below:

$$\boldsymbol{\alpha}_{\mathbf{mol.}} = \boldsymbol{\Phi}_{\mathrm{d}}\boldsymbol{\alpha}_{\mathbf{space}} \tag{2.9}$$

Thus, the interaction potential is expressed by the following formula that contains components of the polarizabiliy tensor in the molecule-fixed frame:

$$V_{\mathrm{p}}(E(t),\theta,\chi) = -\frac{1}{2}[E(t)]^2\big\{\big(\alpha_{xx}-\alpha_{yy}\big)\cos^2\chi\sin^2\theta + \alpha_{yy} + \big(\alpha_{zz}-\alpha_{yy}\big)\cos^2\theta\big\}, \tag{2.10}$$

where χ and θ are Euler angles. This interaction potential does not depend on φ because the laser pulse polarized along the Z axis has cylindrical symmetry. For linear molecules, α_{xx} is equal to α_{yy} when choosing the molecular axis of the linear molecule as the z axis. Therefore, we obtain the final form

$$V_{\mathrm{p}}(E(t),\theta) = -\frac{1}{2}[E(t)]^2\left(\alpha_{\perp}\sin^2\theta + \alpha_{||}\cos^2\theta\right) = -\frac{1}{2}[E(t)]^2(\alpha_{\perp} + \Delta\alpha\cos^2\theta), \tag{2.11}$$

where $\alpha_{\perp} = \alpha_{xx} = \alpha_{yy}$, $\alpha_{||} = \alpha_{zz}$, and $\Delta\alpha = \alpha_{||} - \alpha_{\perp}$. The polarizability anisotropy $\Delta\alpha$ is larger than zero for most linear molecules. As can be seen from Eq. (2.11), the interaction between the intense laser pulse and linear molecule depends on the angle between the molecular axis and polarization direction of the laser pulse, θ.

The typical timescale of rotational motion is about 10^{-12} - 10^{-10} s in the case that linear triatomic molecules are considered. This timescale is much longer than the pulse width of the intense femtosecond laser pulse. Under such conditions, sequence of rotational Raman excitations is induced by the interaction between the molecule and intense femtosecond laser pulse. As a result, several rotational states are coherently populated [117]. In other words, a rotational wave packet is created. Molecular axis aligns along the Z axis in the space-fixed frame periodically under a field-free condition because of the time evolution of the rotational wave packet [90, 91].

The dynamics of the molecular alignment can be investigated by solving the time-dependent Schrödinger equation (TDSE) shown below:

$$i\hbar\frac{\partial}{\partial t}|\psi(t)\rangle = H|\psi(t)\rangle. \tag{2.12}$$

The rotational wave packet $|\psi(t)\rangle$ is expanded in the complete set of rotational eigenstates as

$$|\psi(t)\rangle = \sum_{\mathbf{n}} c_{\mathbf{n}}(t)e^{-i\frac{E_{\mathrm{rot}}(\mathbf{n})}{\hbar}t}|\mathbf{n}\rangle, \tag{2.13}$$

where $\mathbf{n}$ is the collective rotational index, $|\mathbf{n}\rangle$ is the basis function, and $E_{\mathrm{rot}}(\mathbf{n})$ is the rotational energy in units of Joule. Under a rigid-rotor approximation, Hamiltonian is written as

$$H = H_0 + V_{\mathrm{p}}(E(t),\theta) = H_0 - \frac{1}{2}[E(t)]^2(\alpha_{\perp} + \Delta\alpha\cos^2\theta), \tag{2.14}$$

where H_0 is the field-free Hamiltonian. Since $|\mathbf{n}\rangle$ is the eigenstates of the field-free Hamiltonian, $H_0|\mathbf{n}\rangle = E_{\mathrm{rot}}(\mathbf{n})|\mathbf{n}\rangle$ is satisfied. In typical experiments of the molecular alignment, the central wavelength of intense femtosecond laser pulses is 800 nm [7]. The oscillation period of this electric field is 2.7 fs, which is much shorter than the rotational

period of molecules. Hence, it is possible to use the cycle-averaged Hamiltonian given by

$$\bar{H} = H_0 - \frac{1}{4}[\varepsilon(t)]^2(\alpha_\perp + \Delta\alpha\cos^2\theta). \tag{2.15}$$

By substituting Eqs. (2.13) and (2.15) into Eq. (2.12), we obtain

$$\frac{\mathrm{d}c_{\mathbf{n}}(t)}{\mathrm{d}t} = \frac{i}{4\hbar}[\varepsilon(t)]^2\left\{\alpha_\perp c_{\mathbf{n}}(t) + \Delta\alpha\sum_{\mathbf{n}'} d_{\mathbf{n},\mathbf{n}'}c_{\mathbf{n}'}(t)e^{-i\frac{E_{\mathrm{rot}}(\mathbf{n}')-E_{\mathrm{rot}}(\mathbf{n})}{\hbar}t}\right\}, \tag{2.16}$$

where

$$d_{\mathbf{n},\mathbf{n}'} = \langle\mathbf{n}|\cos^2\theta\,|\mathbf{n}'\rangle. \tag{2.17}$$

2.2.2 Selection rules

Selection rules of the rotational Raman excitation are obtained by calculating the matrix elements, $d_{\mathbf{n}'',\mathbf{n}'}$. Appropriate basis functions should be adopted for calculating these matrix elements. For $^1\Sigma^+$ molecules, such as OCS and N_2O, a rotational wave function is expressed by spherical harmonics, $|JM\rangle$. Therefore, the matrix elements of these molecules are expressed by

$$d_{J''M'',J'M'} = \langle J''M''|\cos^2\theta\,|J'M'\rangle, \tag{2.18}$$

The matrix elements above have non-zero values only when $\Delta J = J' - J'' = 0, \pm 2$ and $\Delta M = M' - M'' = 0$. It should be noted that M is preserved when a linearly-polarized laser pulse is used.

In contrast to OCS and N_2O, a different basis function should be used for N_2O^+ ($\tilde{X}\ ^2\Pi$) to calculate the matrix elements. In general, $^2\Pi$ molecules are well described by Hund's coupling case (a) for low-J states. The basis function is

$$|J,|\Omega|,M,p\rangle = \frac{1}{2^{1/2}}\{|J,\Omega,M\rangle + \varepsilon|J,-\Omega,M\rangle\}, \tag{2.19}$$

where $|J,\Omega,M\rangle = |\eta\Lambda;S\Sigma;J,\Omega,M\rangle$ and $\varepsilon = \sigma(-1)^{J-1/2}$ [118]. Here, p represents the total parity, η denotes other quantum numbers required for characterizing the state (e.g., vibrational quantum number), and σ is the symmetry index. The values of σ = +1 and −1 correspond to + and − total parities, respectively.

As J increases, a coupling scheme of angular momenta in $^2\Pi$ states is described by an intermediate representation between case (a) and (b) [119] because the effect of

spin-decoupling becomes considerable at high-J states. Therefore, the basis function is expressed as a linear combination of case (a) basis functions:

$$|JMp; \mathrm{F}_1\rangle = a_J|J, |\Omega| = 1/2, M, p\rangle + b_J|J, |\Omega| = 3/2\,, M, p\rangle \tag{2.20}$$

$$|JMp; \mathrm{F}_2\rangle = -b_J|J, |\Omega| = 1/2, M, p\rangle + a_J|J, |\Omega| = 3/2\,, M, p\rangle \tag{2.21}$$

where

$$a_J = \sqrt{\frac{X + \left(\frac{A}{B} - 2\right)}{2X}}, \tag{2.22}$$

$$b_J = \sqrt{\frac{X - \left(\frac{A}{B} - 2\right)}{2X}}, \tag{2.23}$$

and

$$X = \sqrt{4\left(J + \frac{1}{2}\right) + \frac{A}{B}\left(\frac{A}{B} - 4\right)}. \tag{2.24}$$

The values of $|a_J|^2$ and $|b_J|^2$ for N_2O^+ ($\widetilde{X}\ ^2\Pi$) are calculated using reported molecular constants [110, 113] and represented in Fig. 2.3.

We can calculate the matrix elements, $d_{\mathbf{n}'',\mathbf{n}'}$, using these basis functions and obtain

$$\begin{aligned}\langle J''M''p''; \mathrm{F}_k|\cos^2\theta\,|J'M'p'; \mathrm{F}_i\rangle \\ = \delta_{\sigma''\sigma'}\left\{A_{J''}^{\mathrm{F}_k}A_{J'}^{\mathrm{F}_i}\langle J'', \Omega = 1/2, M''|\cos^2\theta\,|J', \Omega = 1/2, M'\rangle\right. \\ \left. + B_{J''}^{\mathrm{F}_k}B_{J'}^{\mathrm{F}_i}\langle J'', \Omega = 3/2\,, M''|\cos^2\theta\,|J', \Omega = 3/2, M'\rangle\right\},\end{aligned} \tag{2.25}$$

where

$$A_J^{\mathrm{F}_i} = \begin{cases} a_J & (\mathrm{F}_1 \text{ component}) \\ -b_J & (\mathrm{F}_2 \text{ component}) \end{cases} \tag{2.26}$$

and

$$B_J^{\mathrm{F}_i} = \begin{cases} b_J & (\mathrm{F}_1 \text{ component}) \\ a_J & (\mathrm{F}_2 \text{ component}) \end{cases} \tag{2.27}$$

Finally, selection rules are $\Delta J = 0, \pm1, \pm2$, $\Delta M = 0$, and $\sigma' = \sigma''$ ($\pm \leftrightarrow \pm$) because of the conditions that the matrix elements in Eq. (2.25) have non-zero values. Transitions between the F_1 and F_2 components are also allowed. However, probability of such transitions is considerably low because of the large energy difference between these components [120, 121].

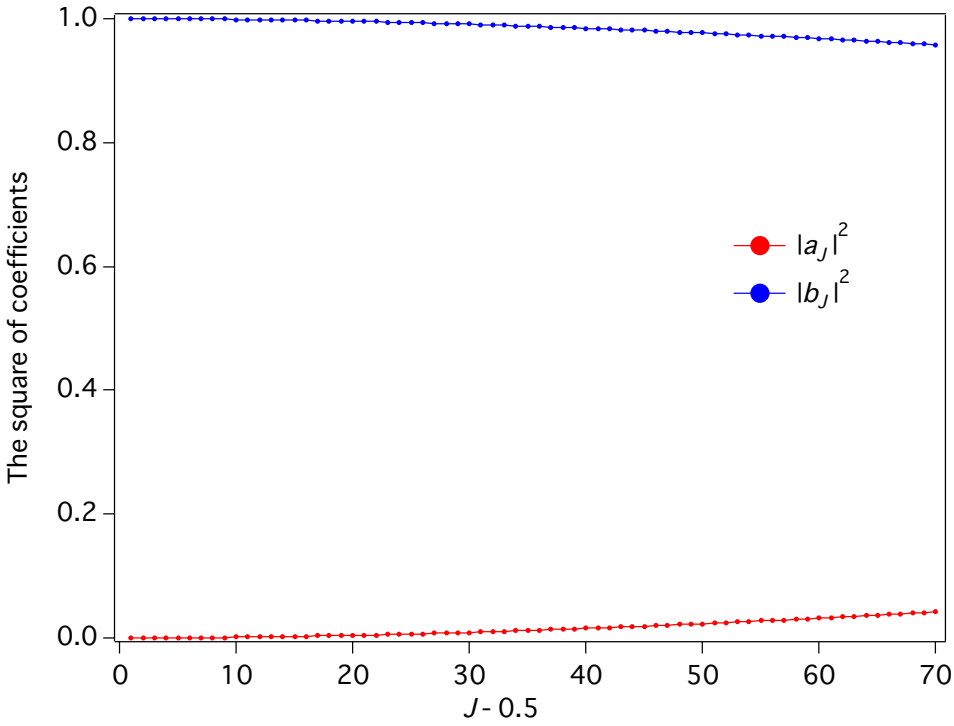

Figure 2.3: Coefficients of basis functions calculated using Eqs. (2.22) and (2.23).

2.2.3 Evaluation of molecular alignment

The degree of molecular alignment can be evaluated by the expectation value of $\cos^2\theta$, i.e., $\langle\cos^2\theta\rangle = \langle\psi(t)|\cos^2\theta|\psi(t)\rangle$. When molecules rotate randomly in gas phase, $\langle\cos^2\theta\rangle$ is equal to 1/3. If molecules align perfectly along the Z axis in the space-fixed frame, $\langle\cos^2\theta\rangle = 1$. In the case that molecular axis distribution is completely localized at $\theta = 0$, $\langle\cos^2\theta\rangle$ equals 0.

If initial rotational states are thermally populated, it is necessary to take a thermal-average as shown below:

$$\langle\langle\cos^2\theta\rangle\rangle = \sum_J \frac{\exp\left[-\frac{E_{\mathrm{rot}}(J)}{k_{\mathrm{B}}T_{\mathrm{rot}}}\right]}{Z_{\mathrm{rot}}} \sum_{M=-J}^{J} \langle\cos^2\theta\rangle_{\mathbf{n}_i}, \tag{2.28}$$

where k_{B} is the Boltzmann constant, T_{rot} is the rotational temperature, Z_{rot} is the rotational partition function, and $\mathbf{n}_{\mathrm{i}}$ stands for collective quantum numbers of the initial rotational eigenstate. It is necessary to prepare rotationally-cooled molecules to achieve the high degree of molecular alignment [90].

2.2.4 Theoretical fundamentals on molecular orientation

In order to prepare oriented molecules, inversion symmetry should be broken by mixing different parities [122]. The total parity of $^1\Sigma^+$ molecules alternates with J as shown in Fig. 2.1. Therefore, the polarizability interaction does not induce transitions that can connect the different parities because of the selection rules ($|\Delta J| = 0, 2$).

The transitions that can connect the different parities are induced via a hyperpolarizability interaction when nonresonant two-color laser pulses, which consist of the fundamental wave with a frequency of ω and its second harmonic, interact with linear molecules [123]. The electric field of the two-color laser pulse polarized along the Z axis is expressed by

$$E(t) = E_\omega(t) + E_{2\omega}(t) = \varepsilon_\omega(t)\cos\omega t + \varepsilon_{2\omega}(t)\cos(2\omega t + \phi_{\mathrm{rel}}). \tag{2.29}$$

where $\varepsilon_\omega(t)$ and $\varepsilon_{2\omega}(t)$ are the envelope functions of the laser pulses and ϕ_{rel} is the relative phase between the fundamental wave and its second harmonic. As shown in Fig. 2.4, the electric field has asymmetric amplitudes when $\phi_{\mathrm{rel}} = k\pi$, where k is integer. In contrast, such asymmetry vanishes when $\phi_{\mathrm{rel}} = (k+1/2)\,\pi$.

Hamiltonian including the field-free Hamiltonian and interaction between the phase-locked two-color laser pulse and linear molecule is written as

$$H = H_0 + V_{\mathrm{d}}(E(t), \theta) + V_{\mathrm{p}}(E(t), \theta) + V_{\mathrm{h}}(E(t), \theta), \tag{2.30}$$

where $V_{\mathrm{d}}(E(t), \theta)$ is the dipole interaction term and $V_{\mathrm{h}}(E(t), \theta)$ is the hyperpolarizability interaction term [123]. The interaction terms, $V_{\mathrm{d}}(E(t), \theta)$ and $V_{\mathrm{h}}(E(t), \theta)$, are given by

$$V_{\mathrm{d}}(E(t), \theta) = -\mu E(t)\cos\theta \tag{2.31}$$

and

$$V_{\mathrm{h}}(E(t), \theta) = -\frac{1}{6}E(t)^3\left\{\left(\beta_{zzz} - 3\beta_{zxx}\right)\cos^3\theta + 3\beta_{zxx}\cos\theta\right\}, \tag{2.32}$$

respectively. By taking a cycle average, we obtain

$$\bar{V}_{\mathrm{d}} = 0 \tag{2.33}$$

and

$$\begin{aligned}\bar{V}_{\mathrm{h}}(t, \theta) = &-\frac{1}{8}\left\{\left(\beta_{zzz} - 3\beta_{zxx}\right)\cos^3\theta + 3\beta_{zxx}\cos\theta\right\} \\ &\times \cos\phi_{\mathrm{rel}}\{\varepsilon_\omega(t)\}^2\{\varepsilon_{2\omega}(t)\}\end{aligned} \tag{2.34}$$

for the dipole and hyperpolarizability interaction terms, respectively. Different selection

rules ($\Delta J = \pm 1, \pm 3$) are allowed because of $\cos\theta$ and $\cos^3\theta$ terms in the hyperpolarizability interaction potential. Transitions associated with these selection rules can connect rotational states with different parities.

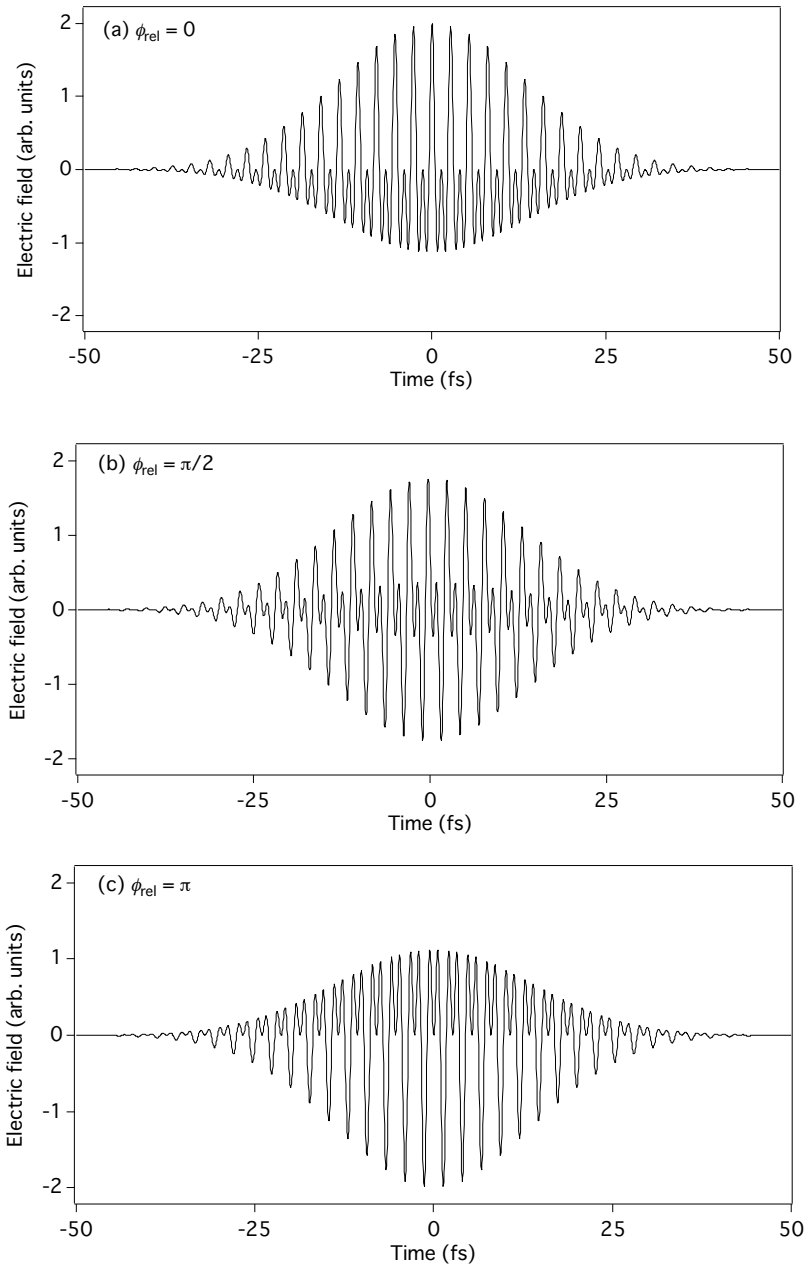

Figure 2.4: Electric fields of phase-locked two-color laser pulses. These electric fields are calculated using Eq. (2.29). The wavelength of the fundamental wave is 800 nm. The maximum amplitudes of the fundamental wave and its second harmonic are assumed to be the same, i.e., $\varepsilon_\omega(t = 0) = \varepsilon_{2\omega}(t = 0) = 1$. (a) $\phi_{rel} = 0$. (b) $\phi_{rel} = \pi/2$. (c) $\phi_{rel} = \pi$.

2.2.5 Evaluation of molecular orientation

The degree of molecular orientation is often evaluated by the expectation value of cosθ, i.e., $\langle \cos\theta \rangle = \langle \psi(t) | \cos\theta | \psi(t) \rangle$. When the number of molecules pointing upward is equal to that of molecules pointing downward, $\langle \cos\theta \rangle$ has the value of 0. If molecular orientation is achieved, $\langle \cos\theta \rangle$ has non-zero values. The sign of $\langle \cos\theta \rangle$ depends on the orientation of molecules.

If initial rotational states are thermally populated, a thermally-averaged expectation value expressed by the following equation should be used.

$$\langle\langle \cos\theta \rangle\rangle = \sum_{J} \frac{\exp\left[-\frac{E_{\mathrm{rot}}(J)}{k_{\mathrm{B}}T_{\mathrm{rot}}}\right]}{Z_{\mathrm{rot}}} \sum_{M=-J}^{J} \langle \cos\theta \rangle_{\mathbf{n}_i} \tag{2.35}$$

Rotational temperature should be lowered to achieve the high degree of the molecular orientation.

Chapter 3

Multiple Ionization of Axis-Controlled OCS Molecules by Intense Femtosecond Laser Pulses

This chapter is not available because the author intends to publish the data presented in this chapter within 5 years.

Chapter 4

Enhancement and Control of Molecular Orientation of OCS by the Alignment-Assisted Method

4.1 Introduction

Considering recent technological advances in generation of attosecond laser pulses [9-11], it is expected that electronic motion in molecular frame will be investigated in detail in near future. One of the most conventional methods of triggering the electronic motion is tunneling ionization [13, 160-162]. An electronic wave packet, which is a superposition of several electronic states, is created in ionic states through this ionization process and evolves with time. From a different point of view, a hole created through the ionization migrates in a molecule [163]. In order to understand this charge migration process in molecular frame, it is necessary to reveal how the tunneling ionization probability depends on the angle between the molecular axis and the laser field because such information is useful to determine the initial position of the hole.

A technique of field-free molecular alignment by nonresonant intense femtosecond laser pulses [90, 91] is one of the most powerful methods for investigating the tunneling ionization process. In fact, it has been found that the tunneling ionization probability of symmetric linear molecules strongly depends on the angle between the polarization direction of the laser pulse and the molecular axis with the aid of this technique [93]. It should be noted that the molecular alignment is sufficient for linear molecules that contain an inversion center. Distinguishing the head and tail of a polar molecule, i.e., control of molecular orientation, is also required for investigating the tunneling ionization in molecular frame.

Unfortunately, the control of molecular orientation is still a challenging task compared to the molecular alignment. In the past decade, various optical techniques for

achieving molecular orientation have been developed [164-171]. Phase-locked two-color intense femtosecond laser pulses, which consist of a fundamental wave and its second harmonic, are frequently used to orient molecules [164, 166, 167, 169]. Two mechanisms of the molecular orientation induced by the two-color intense laser pulses have been investigated theoretically [172] and experimentally [169]. The first mechanism is based on a hyperpolarizability (HP) interaction [123], which is responsible for the molecular orientation when the intensity of the two-color laser pulses is not high enough to induce tunneling ionization of molecules. The molecular orientation is achieved via the hyperpolarizability interaction because this interaction allows parity-breaking rotational transitions (see Chapter 2). On the other hand, when the effect of the tunneling ionization by the two-color intense laser pulses cannot be neglected, an ionization depletion (ID) mechanism, where molecules that point in the specific direction are selectively ionized, is dominant. The higher degree of the molecular orientation can be achieved by the ionization depletion than by the hyperpolarizability interaction [169, 172]. However, the hyperpolarizability interaction is more preferable than the ionization depletion in terms of application to various experiments because the number of density is decreased when the tunneling ionization occurs. Although the technique of the molecular orientation based on the hyperpolarizability interaction has already been applied to a few studies [161, 173], the achieved degree of the molecular orientation is low [164, 174].

In order to increase the degree of the molecular orientation, an alignment-assisted method, in which the two-color laser pulses interact with molecules aligned by an intense laser pulse in advance, has been proposed theoretically [175-177] and demonstrated experimentally [174, 178, 179]. Compared to the conventional experiment on the molecular orientation, in which only the two-color laser pulses are used, the degree of molecular orientation for CO molecules increases by a factor of 2.9 using the alignment-assisted method [174].

One of the most powerful advantages of the alignment-assisted method is that this method has some adjustable laser parameters for controlling molecular orientation because two pump pulses are used. The inversion of molecular orientation has been demonstrated for CO molecules by adjusting a relative phase between the fundamental wave and its second harmonic of the two-color laser pulses [174]. In addition to the relative phase, it is expected that the delay between the two pump pulses also affects

orientation dynamics. However, it has not been investigated experimentally how a change of the delay can be used as a control parameter. Revealing the dependence of the orientation dynamics on the temporal delay is desired for broadening the possibility of controlling molecular orientation.

In this study [180], the enhancement and control of molecular orientation of OCS by the alignment-assisted method is investigated. Conditions for achieving the high degree of molecular orientation are theoretically explored by changing the relative phase of the two-color laser pulses and the delay between the two pump pulses systematically. On the basis of the theoretical predictions, signals of the molecular orientation are measured. In addition to the relative phase of the two-color intense laser pulses, the delay between the two pump pulses is experimentally adjusted to control molecular orientation.

4.2 Experiment

An experimental setup for controlling molecular orientation based on the alignment-assisted method is shown in Fig. 4.1. A linearly polarized femtosecond laser pulse, which has a temporal duration of 100 fs, a central wavelength of 800 nm, and a pulse energy of 8 mJ, is generated from a Ti:sapphire chirped-pulse amplification laser system with a repetition rate of 10 Hz. The first half mirror (HM1) divided the output pulse into a pair of equivalent laser pulses. One of them passed through HM1 and the second half mirror (HM2) and was used as a probe pulse, which induces Coulomb explosion. The laser pulse reflected by HM1 was sent to a beam splitter (BS), at which 30 % of the energy of an incident laser pulse is reflected and the rest of the laser pulse is transmitted. The laser pulse reflected by BS was spatially overlapped with the probe pulse using HM2 and adopted as an alignment pulse. The energy of the alignment pulse was adjusted by changing the diameter of an iris placed in front of HM2. The laser pulse that had passed through BS was sent to a beta barium borate (β-BBO) crystal with a thickness of 200 μm in order to generate the second harmonic. Delay between a fundamental wave (ω) and second harmonic (2ω) caused by the group-velocity-dispersion of the β-BBO crystal and other optical materials was compensated by three calcite plates. One of these calcite plates was mounted on a fine rotation stage to control the relative phase between the fundamental wave and second harmonic. The polarization directions of the fundamental wave and second harmonic were set to be parallel using a wave plate, which works as a half and full wave plate at frequencies of ω and 2ω, respectively. The phase-locked two-color laser pulses, called an orientation pulse, passed through an iris with a diameter of 3.5 mm to avoid tunneling ionization. The temporal delay between the alignment pulse and orientation pulse, τ_1, was fixed to be 20.6 ps and 61.7 ps, which correspond to a quarter and three quarters of a rotational period of OCS, respectively. The delay τ_1 has positive values when molecules are irradiated by the alignment pulse prior to the orientation pulse. The temporal delay between the orientation pulse and probe pulse, τ_2, was controlled by moving mirrors mounted on a motorized linear translation stage (Sigma Koki, KST-(GS)-50X) with a step of 8.0 μm.

Rotationally-cooled molecules were prepared by taking advantage of supersonic

expansion. OCS gas (0.8%) diluted in He gas with a stagnation pressure of 40 atm was expanded into a vacuum chamber equipped with a Wiley-McLaren time-of-flight (TOF) mass spectrometer [144] through a pulsed valve with a repetition rate of 10 Hz. A supersonic molecular beam is prepared after an ejected supersonic flow passes through a skimmer.

The alignment pulse, orientation pulse, and probe pulse were focused onto the supersonic molecular beam by an aluminum-coated concave mirror with a focal length of 200 mm. The axes of laser propagations, the supersonic molecular beam, and a flight axis were mutually perpendicular. Focal intensities of the alignment pulse, orientation pulse, and probe pulse at the interaction region were estimated from the measured beam sizes, pulse energies, pulse duration, and calculation to be $I_A = 1\times10^{13}$ W/cm^2, $I_{O(\omega)} = I_{O(2\omega)} = 2\times10^{13}$ W/cm^2, and $I_{probe} = 6\times10^{14}$ W/cm^2, respectively. The polarization directions of all laser pulses were set to be parallel to the Z axis in the space-fixed frame, which lies along a static electric field applied in the interaction region and points to a michrochannel-plate detector. Ions produced by the probe pulses were accelerated by the static electric field in the interaction region and detected by the microchannel-plate detector. Mass spectra were obtained by recording ion signals as a function of a flight time. Ion yields were obtained by integrating peaks in mass spectra.

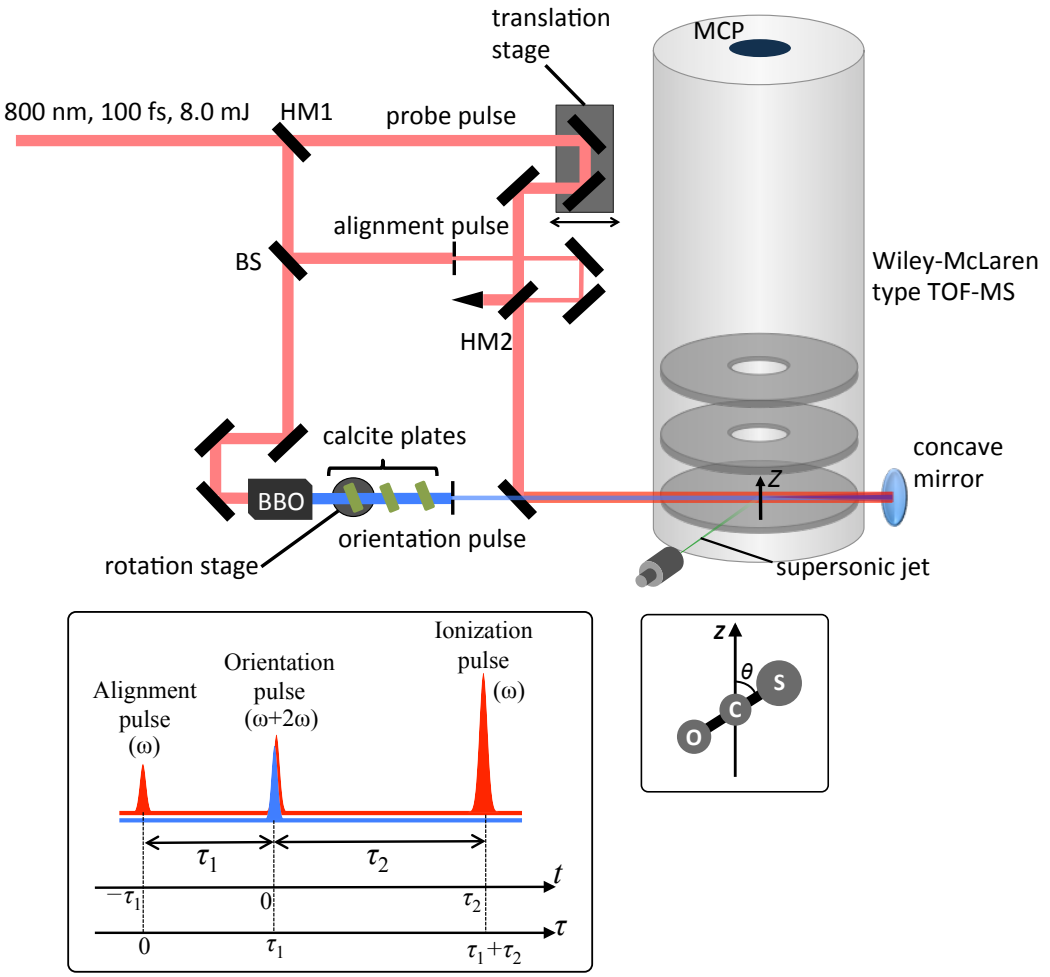

Figure 4.1: Experimental setup and scheme.

4.3 Results and Discussion

An observed mass spectrum shows that many ions, such as S^+, CO^+, S^{2+}, O^+, C^+, S^{3+}, O^{2+}, OCS^+ and OCS^{2+}, are produced by the probe pulse. Doublet peaks are clearly identified for most of the observed fragment ions because of high mass resolution of the TOF mass spectrometer ($m/\Delta m$ = 460). The orientation of OCS against the detector just before the fragmentation can be determined from these doublet peaks because they are originated from fragment ions ejected in the positive and negative directions of the Z axis [144]. As in refs. [170, 181], the doublet peaks of S^{3+} are selected to evaluate the degree of molecular orientation because they are isolated well from other signals of ions in the mass spectrum.

The relative phase ϕ_{rel} between the fundamental wave and the second harmonic forming the orientation pulse is determined by taking advantage of an orientation-selective ionization [152]. The asymmetric electric field of the two-color laser pulses is changed by adjusting ϕ_{rel} as shown in Fig. 2.4. The positive amplitude of the electric field is larger than the negative one when fixing ϕ_{rel} at $2k\pi$, where k is integer (see Fig. 2.4 (a)). In this case, OCS molecules are preferentially ionized when S atom of OCS points to the negative direction of the two-color laser field [152]. On the other hand, when ϕ_{rel} is tuned at $(2k+1)\,\pi$ (see Fig. 2.4 (c)), OCS molecules whose S atom points to the positive direction of the two-color laser field are selectively ionized [152]. When ϕ_{rel} is fixed at $(k+1/2)\,\pi$, the orientation-selective ionization does not occur because the positive and negative amplitudes of the two-color laser field have the same value (see Fig. 2.4 (b)). Therefore, the orientation-selective ionization of OCS can be investigated by measuring the dependence of the ratio $R = Y_f / Y_b$ on ϕ_{rel}, where Y_f and Y_b are the yields of S^{3+} ions ejected in the positive and negative direction of the Z axis, respectively. Figure 4.2 shows the observed dependence of R on the tilt angle of the calcite plate. Only the orientation pulse is used during the experiment on the phase calibration. Other laser pulses are blocked by removable beam dumpers. The iris placed on the optical path of the orientation pulse is removed to induce dissociative ionization. It is found that the ratio R oscillates periodically as a function of the tilt angle. The horizontal axis in Fig. 4.2 can be calibrated because R has minimum at $\phi_{rel} = 2k\pi$. The relative phase ϕ_{rel} is set to be zero in the following experiment, except in an experiment for investigating the dependence of

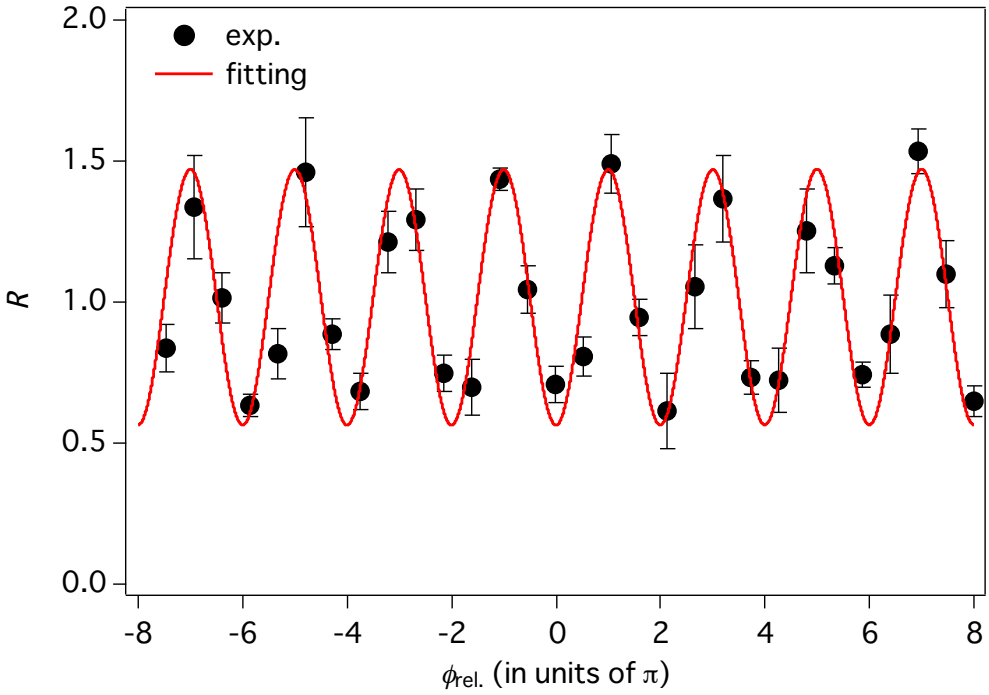

Figure 4.2: The dependence of the yield ratio R on the relative phase, $\phi_{rel.}$

the molecular orientation on $\phi_{rel.}$

In order to track the orientation dynamics of molecules induced by the orientation pulse, the orientation parameter defined by $\eta_O = (Y_f - Y_b) / (Y_f + Y_b)$ is measured as a function of τ_2. When molecules are not oriented, η_O is equal to 0 because Y_f has the same value as Y_b. In contrast, η_O has non-zero value when molecules are oriented. The sign of η_O reflects the orientation of molecules. The dependence of the measured η_O on τ_2 is shown by a black curve in Fig. 4.3 (a). In this experiment, the intensity of the orientation pulse is reduced with the iris in order to avoid tunneling ionization only by this pulse. No distinct peaks are observed in Fig. 4.3 (a), which fact suggests that molecular orientation is not effectively induced by both the orientation pulse and static electric field applied for extracting ions in the TOF mass spectrometer.

Time-dependent Schrödinger equation (TDSE) is numerically solved to find optimal conditions for achieving the high degree of molecular orientation using the alignment pulse and orientation pulse. Under the assumption that an envelope function of laser pulses has a Gaussian shape with a duration of 100 fs, electric fields of the pump pulses are expressed by

$$\boldsymbol{E}(t) = \boldsymbol{E}_{\mathrm{A}}(t) + \boldsymbol{E}_{\mathrm{O}}(t), \tag{4.1}$$

$$\boldsymbol{E}_{\mathrm{A}}(t) = \hat{\mathbf{e}}_z\, \varepsilon_{\mathrm{A}}(t+\tau_1) \cos\big(\omega(t+\tau_1)\big), \tag{4.2}$$

and

$$\boldsymbol{E}_{\mathrm{O}}(t) = \hat{\mathbf{e}}_z\big\{\varepsilon_{\mathrm{O}(\omega)}(t) \cos\omega t + \varepsilon_{\mathrm{O}(2\omega)}(t) \cos(2\omega t + \phi_{\mathrm{rel}})\big\}, \tag{4.3}$$

where $\varepsilon_{\mathrm{A}}(t)$, $\varepsilon_{\mathrm{O}(\omega)}(t)$, and $\varepsilon_{\mathrm{O}(2\omega)}(t)$ are the envelope functions of the laser pulses, and $\hat{\mathbf{e}}_z$ is a unit vector along the Z axis in the space-fixed frame. Intensities of the pump pulses are the same as the experimental conditions. Under a rigid-rotor approximation, Hamiltonian is given by Eq. (2.30). The contribution of the ID mechanism is neglected because the intensity of the orientation pulse at the focal region is not high enough to induce tunneling ionization under our experimental conditions. The polarizabilities and hyperpolarizabilities of OCS are reported to be $\alpha_{\parallel}$ = 54.06 a.u., $\alpha_{\perp}$ = 26.09 a.u., $\beta_{\parallel}$ = −46.3 a.u. and $\beta_{\perp}$ = −60.4 a.u. [151]. TDSE is solved in order to obtain a rotational wave packet expressed by Eq. (2.13). The thermally-averaged expectation value of $\cos\theta$, $\langle\langle\cos\theta\rangle\rangle(t)$, is calculated using the obtained rotational wave packet and Eq. (2.35). Rotational temperature is fixed at 25 K because calculated results at this temperature give the best agreement with experimental results. Rotational temperature and laser intensities are fixed during the calculation. The time when the envelope of the orientation pulse reaches the maximum is chosen as a time origin. Hence, t corresponds to τ_2.

Maximum values of $|\langle\langle\cos\theta\rangle\rangle(t)|$ are plotted at different τ_1 and ϕ_{rel} in Fig. 4.4. The horizontal axis of this two-dimensional map is shown in units of τ_{rot}, where τ_{rot} is the rotational period of OCS given by $\tau_{\mathrm{rot}} = h/2B$ = 82.2 ps (see Chapter 3). The delay τ_1 and relative phase ϕ_{rel} are changed with a step of 0.2 τ_{rot} and 0.1 π, respectively. The calculated two-dimensional map in Fig. 4.4 clearly shows that the maximum degree of the molecular orientation is achieved at (τ_1, ϕ_{rel}) = (1/4 τ_{rot}, 0), (1/4 τ_{rot}, 0), (3/4 τ_{rot}, π), and (1/4 τ_{rot}, π).

Based on the calculated results, the dependence of η_{O} on τ_2 is measured with τ_1 and ϕ_{rel} fixed at 3/4 τ_{rot} and 0, respectively. The measured η_{O} shown by a black curve in Fig. 4.3 (b) has a transient signal having a large amplitude originated from the molecular orientation at τ_2 = 41.1 ps, which corresponds to a half of the rotational period. This result shows that the degree of the molecular orientation can be increased by shining the orientation pulse on molecules aligned by the alignment pulse.

According to the two-dimensional map in Fig. 4.4, the high degree of molecular

orientation can be achieved even when changing ϕ_{rel} from 0 to π with τ_1 fixed at 3/4 τ_{rot}. In order to verify it experimentally, the dependence of η_O on τ_2 is measured with ϕ_{rel} tuned at π and shown by a thin red curve in Fig. 4.5. The signal η_O obtained under the condition of ϕ_{rel} = 0 is also shown by a thin blue curve as a reference. Comparing the thin

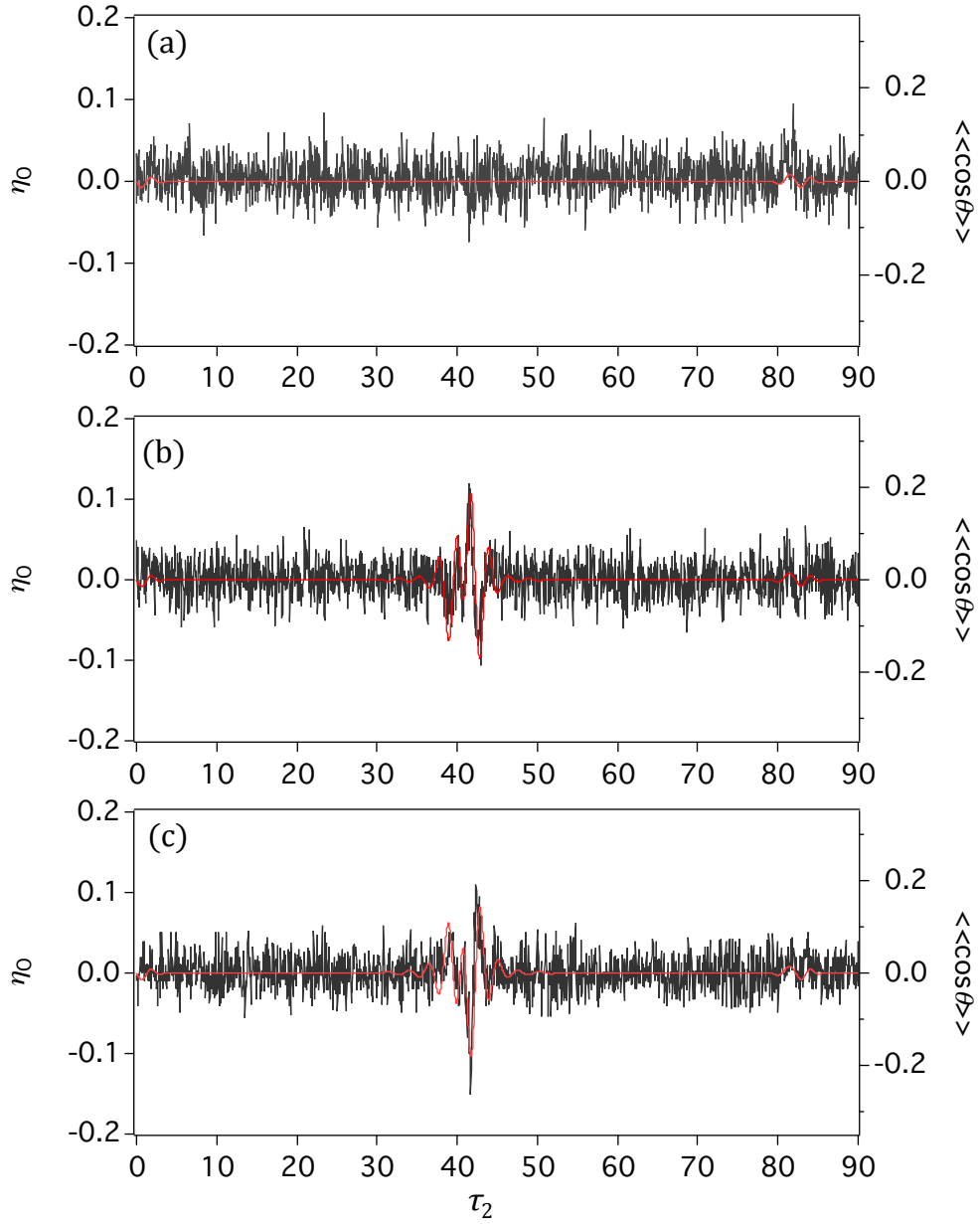

Figure 4.3: The dependence of the orientation parameter on the delay τ_2 (ϕ_{rel} = 0). The measured η_O and calculated $\langle\langle \cos\theta \rangle\rangle$ are shown by black and red curves, respectively. (a) Only the two-color laser pulses are used as the pump pulse. (b) The alignment-assisted method (τ_1 = 3/4 τ_{rot}). (c) The alignment-assisted method (τ_1 = 1/4 τ_{rot}).

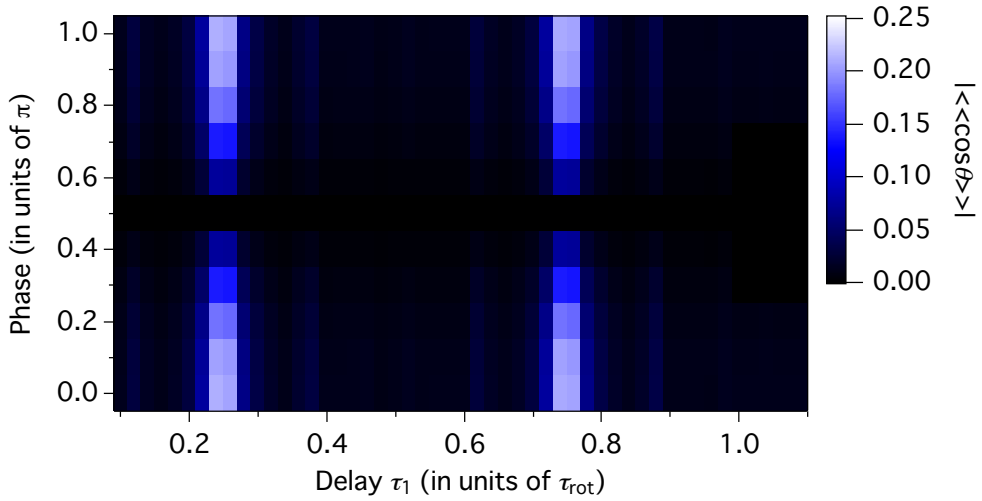

Figure 4.4: The maximum values of the calculated $|\langle\langle\cos\theta\rangle\rangle|$. These values are calculated at various sets of the relative phase ϕ_{rel} and delay τ_1.

blue curve ($\phi_{rel} = 0$) with the thin red one ($\phi_{rel} = \pi$) shows that η_O is inverted by changing ϕ_{rel} from 0 to π even though the absolute values of amplitude are almost the same. The inversion of the measured signals is originated from a change of the molecular orientation. This experimental result verifies that the high degree of the molecular orientation can be achieved at $\phi_{rel} = 0$ and π once τ_1 is fixed at the best delay.

The two-dimensional map in Fig. 4.4 shows that the high degree of the molecular orientation is achieved not only at 3/4 τ_{rot}, but also at 1/4 τ_{rot}. However, it has not been investigated experimentally how changing τ_1 from 3/4 τ_{rot} to 1/4 τ_{rot} affects the dynamics of the molecular orientation. The measured η_O under the condition of (τ_1, ϕ_{rel}) = (1/4 τ_{rot}, 0) is shown by a black curve in Fig. 4.3 (c). A clear oscillatory signal with a large amplitude is observed at τ_2 = 41.1 ps, which is a half of the rotational period of OCS. This result shows that molecules can be strongly oriented by shining the alignment pulse prior to the orientation pulse on molecules with an appropriate delay. Interestingly, the observed signal is inverted by changing τ_1 from 3/4 τ_{rot} to 1/4 τ_{rot}. It should be noted that the inversion of the head-to-tail order is not due to changing ϕ_{rel} by π as shown in Fig. 4.5, but due to adjusting the delay between the alignment pulse and orientation pulse.

Since the calculated $\langle\langle\cos\theta\rangle\rangle(t)$ and measured η_O for S^{3+} behave in the same way [170, 181], it is possible to compare the experimental results with simulated ones. A red curve in Fig. 4.3 (a) is $\langle\langle\cos\theta\rangle\rangle(t)$ calculated under the condition that molecules interact

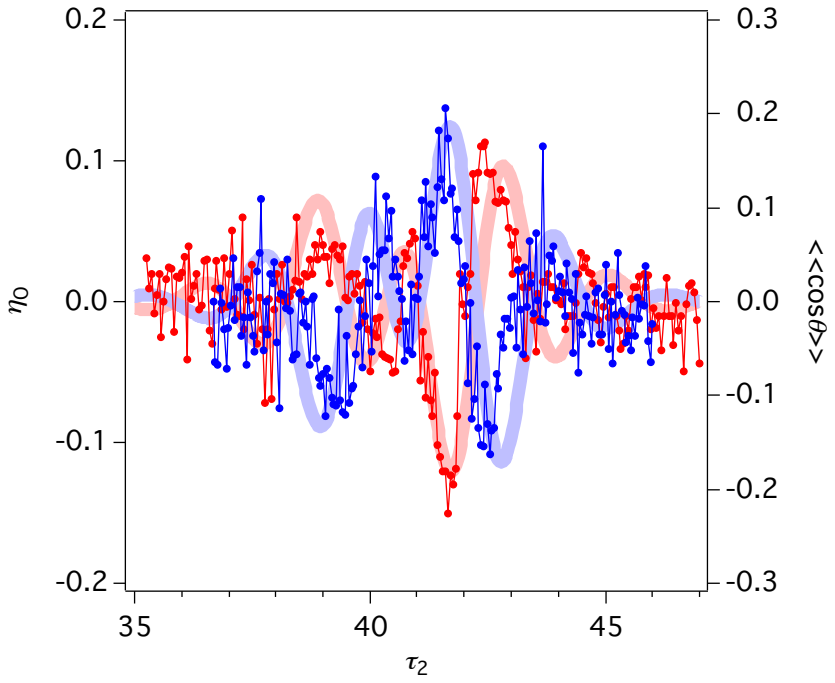

Figure 4.5: The dependences of the measured η_O and calculated $\langle\langle\cos\theta\rangle\rangle$ on the relative phase ϕ_{rel} with τ_1 fixed at 3/4 τ_{rot}. Thin blue curve: experiment (ϕ_{rel} = 0). Thin red curve: experiment (ϕ_{rel} = π). Thick blue curve: calculation (ϕ_{rel} = 0). Thick red curve: calculation (ϕ_{rel}= π).

only with the orientation pulse. Although small oscillation can be seen around t = 82.2 ps, the maximum degree of the molecular orientation is only $|\langle\langle\cos\theta\rangle\rangle(t = 81.5\text{ ps})|$ = 1.5×10^{-2}. The sensitivity of our experimental apparatus to the orientation parameter is not high enough to evaluate this low degree of the molecular orientation as shown by a black curve in Fig. 4.3 (a). Red curves in Figs. 4.3 (b) and (c) show the calculated values of $\langle\langle\cos\theta\rangle\rangle(t)$ on the basis of the alignment-assisted method. As can be seen from the figures, the calculated results agree well with the observed signals. In addition to the observed dependence of η_O on τ_1, the dependence of η_O on ϕ_{rel} is also reproduced by the calculations as shown in Fig. 4.5. The good agreement between the calculated results and the observed signals indicates that the observed molecular orientation is not induced by the ionization depletion, but by the hyperpolarizability interaction.

The low degree of the molecular orientation achieved only by the orientation pulse is due to the thermal averaging over the initial rotational-state distribution as discussed in

a previous study [175]. In order to check the contribution of the thermal averaging, the expectation values,

$$\langle \cos\theta \rangle_{\text{even}}(t) = {}_{\mathbf{n}_{\text{even}}}\langle \psi(t) | \cos\theta | \psi(t) \rangle_{\mathbf{n}_{\text{even}}} \tag{4.4}$$

and

$$\langle \cos\theta \rangle_{\text{odd}}(t) = {}_{\mathbf{n}_{\text{odd}}}\langle \psi(t) | \cos\theta | \psi(t) \rangle_{\mathbf{n}_{\text{odd}}}, \tag{4.5}$$

are calculated numerically, where $|\psi(t)\rangle_{\mathbf{n}_{\text{even}}}$ and $|\psi(t)\rangle_{\mathbf{n}_{\text{odd}}}$ are the rotational wave packets created from initial rotational states with even and odd J, respectively. The thermally-averaged expectation values, $\langle\langle \cos\theta \rangle\rangle_{\text{even}}(t)$ and $\langle\langle \cos\theta \rangle\rangle_{\text{odd}}(t)$, are shown by a blue and red curve in Fig. 4.6 (a), respectively. Clear peaks appear around a half of the rotational period for both $\langle\langle \cos\theta \rangle\rangle_{\text{even}}(t)$ and $\langle\langle \cos\theta \rangle\rangle_{\text{odd}}(t)$. However, $\langle\langle \cos\theta \rangle\rangle_{\text{even}}(t)$ and $\langle\langle \cos\theta \rangle\rangle_{\text{odd}}(t)$ are in antiphase relation. As a result, they cancel each other out.

It should be noted that orientation signals for CO molecules have been observed in a previous study [174] even though only two-color laser pulses, whose intensity is not high enough to ionize molecules, are used. Under the experimental condition in ref. [174], rotational temperature is low enough to make the ratio of populations of rotational states with odd J and even J, $P_{J_{\text{odd}}}/P_{J_{\text{even}}}$, deviate from unity. As a result, $\langle\langle \cos\theta \rangle\rangle_{\text{even}}(t)$ and $\langle\langle \cos\theta \rangle\rangle_{\text{odd}}(t)$ do not have the same absolute values at a half of the rotational period. For CO molecules, $P_{J_{\text{odd}}}/P_{J_{\text{even}}}$ is not equal to 1 when the rotational temperature is lower than 5 K [174]. Since OCS molecules are heavier than CO molecules, lower rotational temperature is required to achieve $P_{J_{\text{odd}}}/P_{J_{\text{even}}} < 1$. Figure 4.7 (a) shows the ratio $P_{J_{\text{odd}}}/P_{J_{\text{even}}}$ calculated as a function of the rotational temperature T_{rot}. The ratio $P_{J_{\text{odd}}}/P_{J_{\text{even}}}$ is unity if the rotational temperature is higher than 0.8 K. The dependence of $\langle\langle \cos\theta \rangle\rangle(t)$ on the rotational temperature is represented in Fig. 4.7 (b). Although the high degree of molecular orientation is achieved around t = 41.1 ps when only the lowest rotational state is populated (T_{rot} = 0.0 K), the maximum value of $|\langle\langle \cos\theta \rangle\rangle(t)|$ decreases rapidly as the rotational temperature increases. This is because $P_{J_{\text{odd}}}/P_{J_{\text{even}}}$ becomes large and is close to unity when $T_{\text{rot}} > 0.5$ K, which results in the cancelation of $\langle\langle \cos\theta \rangle\rangle_{\text{even}}(t)$ and $\langle\langle \cos\theta \rangle\rangle_{\text{odd}}(t)$ as shown in Fig. 4.6 (a).

The alignment-assisted method has been proposed to reduce the effect of the cancellation between $\langle\langle \cos\theta \rangle\rangle_{\text{even}}(t)$ and $\langle\langle \cos\theta \rangle\rangle_{\text{odd}}(t)$ [175]. This scheme takes advantage of the nonadiabatic molecular alignment prior to the molecular orientation. For

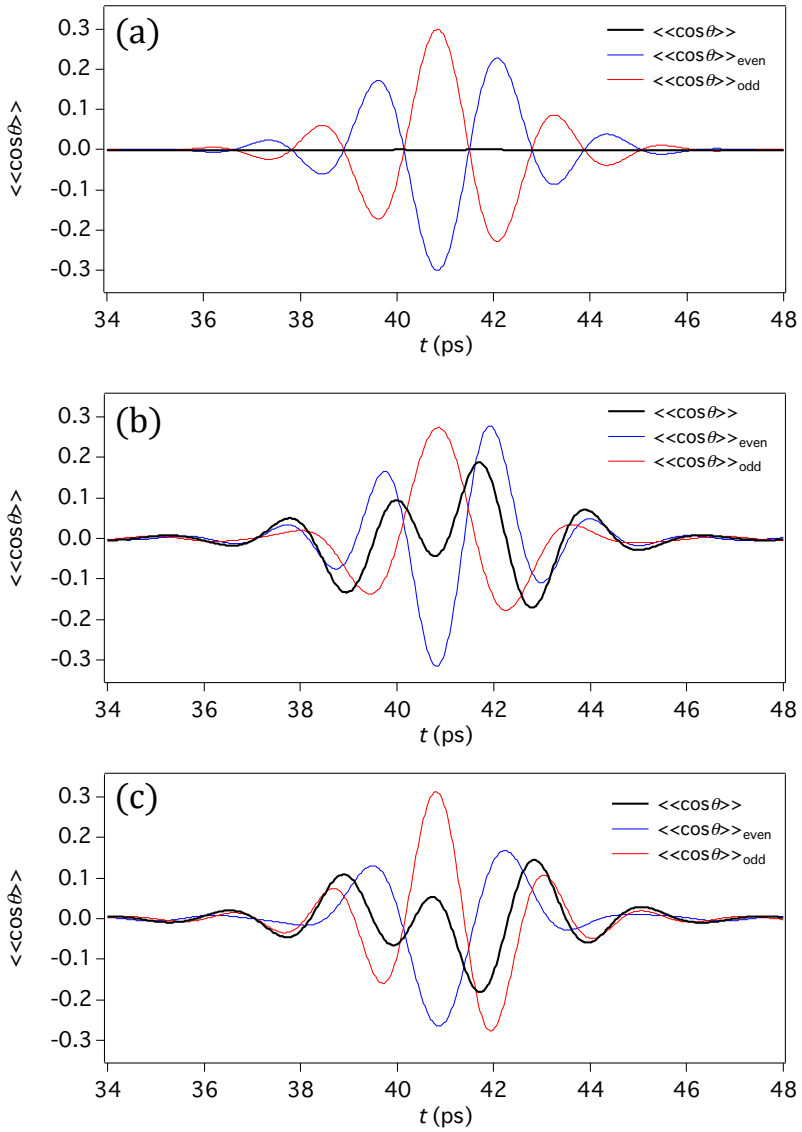

Figure 4.6: The calculated $\langle\langle\cos\theta\rangle\rangle$, $\langle\langle\cos\theta\rangle\rangle_{\text{even}}$, and $\langle\langle\cos\theta\rangle\rangle_{\text{odd}}$. The relative phase ϕ_{rel} is fixed at 0. (a) Only the two-color laser pulses are used as the pump pulse. (b) The alignment-assisted method (τ_1 = 3/4 τ_{rot}). (c) The alignment-assisted method (τ_1 = 1/4 τ_{rot}).

the sake of simplicity, the time τ, which is defined by $\tau = t + \tau_1$, is used to describe the time evolution of the rotational wave packet created by the alignment pulse (see Fig. 4.1). The origin of the time, i.e., $\tau = 0$, is the time when the envelope function of the alignment pulse reaches a maximum. Interaction between the alignment pulse and OCS molecules creates a rotational wave packet via a series of coherent rotational Raman excitations. The created rotational wave packet can be divided into $|\psi(\tau)\rangle_{\mathbf{n}_{\text{odd}}}$ and $|\psi(\tau)\rangle_{\mathbf{n}_{\text{even}}}$ that

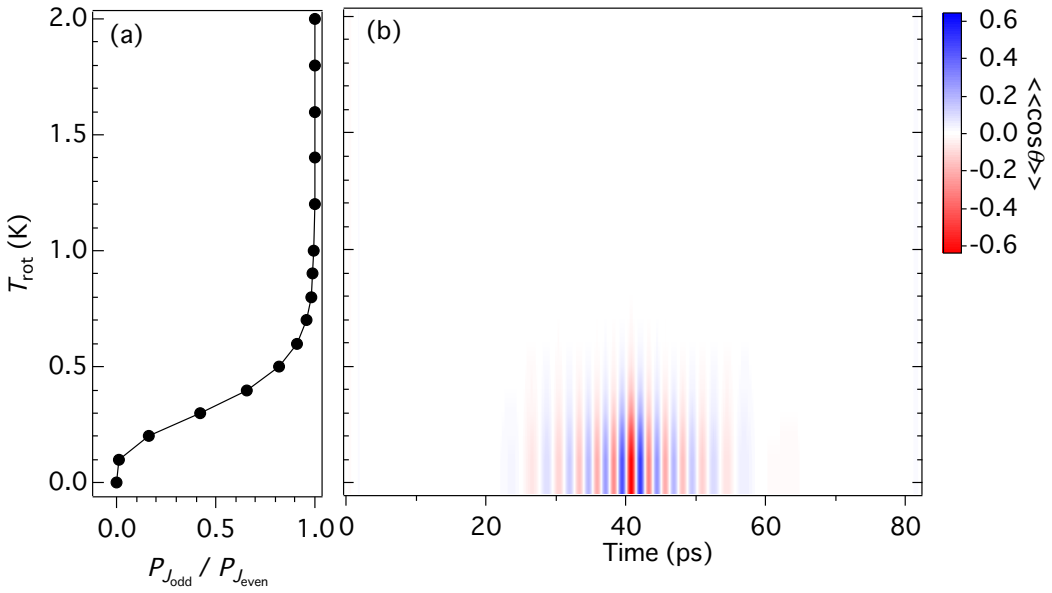

Figure 4.7: The dependence of the population and $\langle\langle\cos\theta\rangle\rangle$ on the rotational temperature, T_{rot}. (a) The ratio of rotational-state population, $P_{J_{odd}}/P_{J_{even}}$. (b) The calculated $\langle\langle\cos\theta\rangle\rangle$ ($\phi_{rel} = 0$).

consist of rotational eigenstates with − and + total parities, respectively. Since the hyperpolarizability interaction depends on θ (see Eq. (2.32)), it is reasonable to discuss the rotational excitation by the orientation pulse based on molecular axis distribution. Here, the molecular axis distributions that are associated with the rotational wave packets $|\psi(\tau)\rangle_{\mathbf{n}_{odd}}$ and $|\psi(\tau)\rangle_{\mathbf{n}_{even}}$ are denoted by $f_{odd}(\theta, \tau)$ and $f_{even}(\theta, \tau)$, respectively. Both $f_{odd}(\theta, \tau)$ and $f_{even}(\theta, \tau)$ localize along the Z axis at $\tau = 1/2\ \tau_{rot}$ and τ_{rot}, which correspond to a half and full revival, respectively. As a result, both of the rotational wave packets interact with the orientation pulse in the same manner at these times. Therefore, if τ_1 is set to be $1/2\ \tau_{rot}$ or τ_{rot}, $\langle\langle\cos\theta\rangle\rangle_{even}(t)$ and $\langle\langle\cos\theta\rangle\rangle_{odd}(t)$ cancel each other out at $t = 1/2\ \tau_{rot}$, which results in low $\langle\langle\cos\theta\rangle\rangle(t)$. In fact, the two-dimensional map in Fig. 4.4 does not show that the high degree of the molecular orientation is achieved at $\tau_1 = 1/2\ \tau_{rot}$ and τ_{rot}.

In contrast to the alignment dynamics at $\tau = 1/2\ \tau_{rot}$ and τ_{rot}, a different behavior can be seen at $\tau = 3/4\ \tau_{rot}$. At this time, $f_{even}(\theta, \tau)$ localizes along the Z axis while $f_{odd}(\theta, \tau)$ is restricted mainly on the X-Y plane. Considering the angular dependence of the hyperpolarizability interaction, only the rotational wave packet $|\psi(\tau)\rangle_{\mathbf{n}_{even}}$ can interact

with the orientation pulse effectively at this time. As a result, molecular orientation is achieved at t = 1/2 τ_{rot} because $\langle\langle\cos\theta\rangle\rangle_{even}(t)$ surpasses $\langle\langle\cos\theta\rangle\rangle_{odd}(t)$. The calculated $\langle\langle\cos\theta\rangle\rangle_{even}(t)$, $\langle\langle\cos\theta\rangle\rangle_{odd}(t)$, and $\langle\langle\cos\theta\rangle\rangle(t)$ are shown in Fig. 4.6 (b). Here, τ_1 is fixed at 3/4 τ_{rot}. Since the cancelation between $\langle\langle\cos\theta\rangle\rangle_{even}(t)$ and $\langle\langle\cos\theta\rangle\rangle_{odd}(t)$ is insufficient, $\langle\langle\cos\theta\rangle\rangle(t)$ has a large amplitude. The oscillation pattern of $\langle\langle\cos\theta\rangle\rangle(t)$ is similar to that of $\langle\langle\cos\theta\rangle\rangle_{even}(t)$. It indicates that the contribution of $|\psi(t)\rangle_{\mathbf{n}_{even}}$ to the orientation dynamics is larger than that of $|\psi(t)\rangle_{\mathbf{n}_{odd}}$.

At τ = 1/4 τ_{rot}, $f_{odd}(\theta, \tau)$ is almost restricted around the Z axis. On the other hand, $f_{even}(\theta, \tau)$ is almost localized at θ = 90°. Therefore, the interaction between the orientation pulse and the molecules at this time results in the enhancement of $\langle\langle\cos\theta\rangle\rangle_{odd}(t)$. In other words, the contribution of $\langle\langle\cos\theta\rangle\rangle_{odd}(t)$ to the orientation dynamics is increased if τ_1 is fixed at 1/4 τ_{rot}. Figure 4.6 (c) shows the calculated results of $\langle\langle\cos\theta\rangle\rangle_{even}(t)$, $\langle\langle\cos\theta\rangle\rangle_{odd}(t)$, and $\langle\langle\cos\theta\rangle\rangle(t)$. The effect of the cancelation between $\langle\langle\cos\theta\rangle\rangle_{even}(t)$ and $\langle\langle\cos\theta\rangle\rangle_{odd}(t)$ is reduced because the contribution of $\langle\langle\cos\theta\rangle\rangle_{odd}(t)$ is larger than $\langle\langle\cos\theta\rangle\rangle_{even}(t)$. As a result, the molecular orientation is achieved.

In addition to the analysis of the orientation dynamics, it is also important to evaluate the enhancement of the molecular orientation quantitatively. When the alignment-assisted method is used, the maximum values of $|\langle\langle\cos\theta\rangle\rangle(t)|$ with τ_1 fixed at 1/4 τ_{rot} and 3/4 τ_{rot} are 0.18 and 0.19, respectively. These maximum values are about 12 times larger than the maximum $|\langle\langle\cos\theta\rangle\rangle(t)|$ achieved under the condition that the alignment pulse is absent. Although the value of $|\langle\langle\cos\theta\rangle\rangle(t)|$ is frequently used for the evaluation of the molecular orientation, it is difficult to understand intuitively how many molecules point in the positive direction of the Z axis based on this parameter. Thus, the normalized molecular axis distribution f (θ) is calculated at the time when the $|\langle\langle\cos\theta\rangle\rangle(t)|$ has a maximum value. A probability of finding molecular axes in the range from θ_L to θ_U is determined by

$$P(\theta_L,\theta_U) = 2\pi \int_{\theta_L}^{\theta_U} f(\theta) \sin\theta \, d\theta \tag{4.6}$$

Since f (θ) is normalized, $P(0, \pi) = 1$ is always satisfied. The probability of finding OCS molecules whose S atoms point in the positive direction of the Z axis is $P(0, 1/6\pi) = 0.15$ at τ_2 = 41.7 ps when the τ_1 is tuned at 3/4 τ_{rot}. This value is 3.9 times larger than the probability of finding molecules pointing in the negative direction, $P(5/6\pi, \pi) = 0.038$.

Such asymmetric distribution is visualized in Fig. 4.8 (a). In contrast to Fig. 4.8 (a), it is clearly seen that the molecular orientation is inverted when the τ_1 is tuned at 1/4 τ_{rot} as shown in Fig. 4.8 (b). Since $P(0, 1/6\pi)$ and $P(5/6\pi, \pi)$ are equal to 0.049 and 0.16, respectively, the number of OCS molecules pointing in the negative direction is 3.3 times larger than that of molecules pointing in the opposite direction.

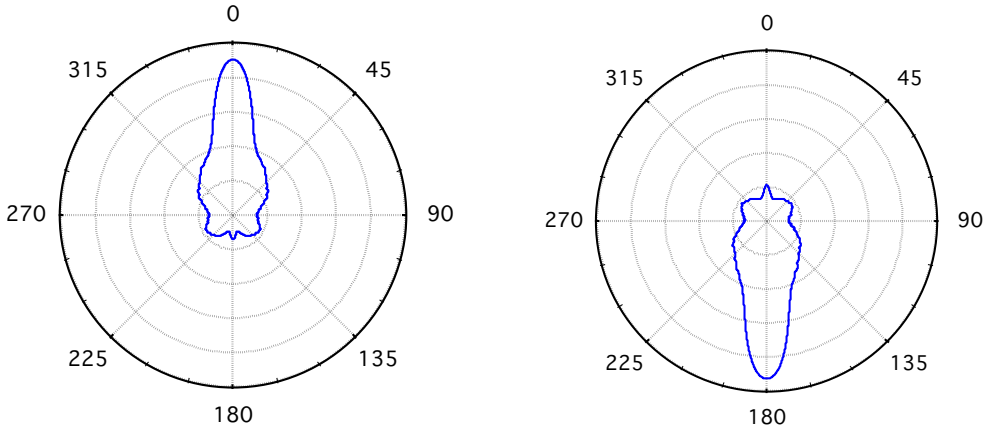

(a) (b)

Figure 4.8: The calculated molecular axis distribution (ϕ_{rel} = 0). (a) τ_1 = 3/4 τ_{rot}, τ_2 = 41.7 ps. (b) τ_1 = 1/4 τ_{rot}, τ_2 = 41.7 ps.

4.4 Conclusion

In this study [180], the enhancement and control of the field-free molecular orientation of OCS molecules is investigated. The signals of the molecular orientation are not observed when only the orientation pulse is used. The TDSE calculation is systematically carried out at various sets of the relative phase ϕ_{rel} and delay τ_1 in order to achieve the high degree of the molecular orientation. It is theoretically shown that molecules are strongly oriented by adjusting ϕ_{rel} and τ_1 appropriately. On the basis of the theoretical predictions, signals of the molecular orientation are observed using the alignment-assisted method. The molecular orientation is achieved via the hyperpolarizability interaction because the measured orientation parameter η_{O} agrees well with the calculated $\langle\langle\cos\theta\rangle\rangle(t)$. The experimentally-achieved value of the highest $|\langle\langle\cos\theta\rangle\rangle(t)|$ is determined by comparing the measured orientation parameter η_{O} with the calculated $\langle\langle\cos\theta\rangle\rangle(t)$. The absolute value of $\langle\langle\cos\theta\rangle\rangle(t)$ is about 12 times larger than that of $\langle\langle\cos\theta\rangle\rangle(t)$ achieved only by the two-color intense laser pulses. The molecular orientation of OCS is inverted by changing ϕ_{rel} from 0 to π. In addition, it is experimentally shown for the first time that the molecular orientation is inverted by changing τ_1 from 1/4 τ_{rot} to 3/4 τ_{rot}. The results presented here broaden the possibility of controlling the molecular orientation.

Chapter 5

Spectroscopic Studies on Strong-Field Ionization of N_2O Molecules

This chapter is not available because the author intends to publish the data presented in this chapter within 5 years.

Chapter 6

Conclusion

The main goal of this thesis is to reveal the ionization of molecules by intense femtosecond laser pulses. In order to achieve this goal, three experiments are conducted.

In the first work of this thesis, double- and triple-ionization processes of axis-controlled OCS molecules induced by the intense femtosecond laser pulses are investigated using a pump-probe method, in which the pump pulse creates a rotational wave packet and the probe pulse induces multiple ionization. The ions generated by the probe pulses are detected by a time-of-flight mass spectrometer. The yields of the observed OCS^{2+} and OCS^{3+} measured as a function of the delay between the pump and probe pulses, τ, oscillate periodically. In the measured dependence of the OCS^{2+} yield on τ, strong transient signals are clearly observed at τ = 41.1 ps and 82.2 ps. The observed strong oscillatory signals are attributed to the time evolution of the created rotational wave packet because these signals appear at fractions of the rotational period of OCS in the electronic and vibrational ground state (τ_{rot} = 82.2 ps). In addition to the strong transient signals, weak transient signals are also observed at τ = 1/6 τ_{rot}, 1/4 τ_{rot}, 1/3 τ_{rot}, 2/3 τ_{rot}, 3/4 τ_{rot}, and 5/6 τ_{rot}. These weak transient signals are assigned to high-order fractional revival structures. In addition to the revival structures observed in the signals of OCS^{2+}, the dependence of the OCS^{3+} yield on τ shows higher-order fractional revival structures at τ = 1/8 τ_{rot}, 3/8 τ_{rot}, 5/8 τ_{rot}, and 7/8 τ_{rot}.

The time-dependent Schrödinger equation (TDSE) is numerically solved to reproduce the observed dependence of the OCS^{2+} and OCS^{3+} yields on τ. The dynamics of the created rotational wave packet and the dependences of the double- and triple-ionization probabilities on the angle between the polarization direction of the probe pulse and the molecular axis of OCS, θ, are taken into account in the calculations. The angular dependences of the double- and triple-ionization probabilities, which are denoted by $W_2(\theta)$ and $W_3(\theta)$, respectively, are expanded by the Wigner D matrix elements with

unknown expansion coefficients. These expansion coefficients are determined by comparing the observed revival structures with the calculated results. The determined $W_2(\theta)$ and $W_3(\theta)$ show that OCS^{2+} and OCS^{3+} are preferably produced when the polarization direction of the probe pulse and molecular axis of OCS are set to be mutually perpendicular. The similar tendency has been already found in the single-ionization process of OCS. The angular dependence of the single-ionization probability, $W_1(\theta)$, that has a large maximum at $\theta = 90°$, was well explained using the tunneling ionization theory including the spatial information of the HOMO and effects of Stark shift and barrier-suppression ionization. The large maxima of $W_1(\theta)$, $W_2(\theta)$, and $W_3(\theta)$ at $\theta = 90°$ are attributed to the fact that OCS^+, OCS^{2+}, and OCS^{3+} are produced by removing electrons from the HOMO of OCS (3π orbital), which is occupied by four electrons. The ejection of electrons from the HOMO in the double- and triple-ionization processes is consistent with that the determined $W_3(\theta)$ is sharper and more complex than $W_2(\theta)$.

The determined $W_2(\theta)$ and $W_3(\theta)$ include higher-order Wigner D matrix elements. It is found that the high-order fractional revival structures observed in the signals of OCS^{2+} and OCS^{3+} yields are originated from these high-order D matrix elements. The contribution of the high-order D matrix elements is an important factor of a sensitive method for probing the molecular axis distribution.

The second work of this thesis is about the enhancement and control of molecular orientation of OCS molecules, which is a desired technique for investigating ionization of polar molecules. First, a well-known method of orienting molecules, in which polar molecules are irradiated with phase-locked two-color intense laser pulses consisting of the fundamental wave with a central frequency of ω and its second harmonic, is adopted. Under our experimental conditions, signals of molecular orientation are not observed within experimental uncertainty. The TDSE calculation shows that the degree of the molecular orientation is only $|\langle\langle\cos\theta\rangle\rangle(t)| = 0.015$, where the double brackets denote the thermally-averaged expectation value and θ is the angle between the polarization direction of the two-color laser pulses and the molecular axis of OCS. In order to achieve the high degree of the molecular orientation, an intense femtosecond laser pulse with a central frequency of ω and the two-color intense laser pulses are used as pump pulses. The TDSE calculation is systematically carried out at various sets of the relative phase of the two-color laser pulses, ϕ_{rel}, and the delay between the two pump pulses, τ_1. It is

theoretically found that strongly-oriented molecules can be prepared by adjusting ϕ_{rel} and τ_1 appropriately. On the basis of the theoretical predictions, the signals of the molecular orientation are experimentally observed under the conditions of (ϕ_{rel}, τ_1) = (0, $1/4\tau_{rot}$), (0, $3/4\tau_{rot}$), and (π, $3/4\tau_{rot}$). It is possible to determine the experimentally-achieved value of the highest $|\langle\langle\cos\theta\rangle\rangle|$ because the observed signals agree well with the calculated $\langle\langle\cos\theta\rangle\rangle$. The absolute value of $\langle\langle\cos\theta\rangle\rangle$ is about 12 times larger than that of $\langle\langle\cos\theta\rangle\rangle$ achieved only by the two-color intense laser pulses. The molecular orientation of OCS is inverted by changing ϕ_{rel} from 0 to π. In addition, it is experimentally shown for the first time that the delay between the two pump pulses can be used as a parameter for controlling the molecular orientation. The orientation of molecules is inverted by changing τ_1 from $3/4\ \tau_{rot}$ to $1/4\ \tau_{rot}$.

In the last part of this thesis, ionization of N_2O molecules induced by intense femtosecond laser pulses is investigated using a spectroscopic technique. In order to reveal the vibrational- and rotational-state distributions of N_2O^+ in the electronic ground state produced by the intense femtosecond laser pulses, the $\tilde{A}\ ^2\Sigma^+$ - $\tilde{X}\ ^2\Pi$ excitation spectra are recorded by measuring the yield of NO^+ generated via the predissociaion process in the $\tilde{A}\ ^2\Sigma^+$ state as a function of excitation wavenumber of nanosecond laser pulses. It is concluded that the vibrational ground state of N_2O^+ ($\tilde{X}\ ^2\Pi$) is predominantly populated by the strong-field ionization of N_2O because only transitions from the vibrational ground state of this molecular ion are observed. The determined vibrational-state distribution of N_2O^+ ($\tilde{X}\ ^2\Pi$) is almost the same as the distribution predicted from Franck-Condon factors (FCFs) for the transitions between the vibrational ground state of N_2O ($\tilde{X}\ ^1\Sigma^+$) and various vibrational states of the molecular ions in the electronic ground state. The similarity between the observed vibrational-state distribution and the FCFs indicates that structural deformation is not induced by the intense femtosecond laser pulses. In addition, it is suggested that the dependence of the tunneling ionization rate on the structures of N_2O and N_2O^+ is negligible.

In order to investigate the rotational-state distribution of N_2O^+ in the electronic and vibrational ground state, $\tilde{X}\ ^2\Pi_{3/2}$ (000), rotationally-resolved excitation spectra of the $\tilde{A}\ ^2\Sigma^+$ (200) - $\tilde{X}\ ^2\Pi_{3/2}$ (000) band are measured and analyzed. The observed spectral patterns show clear dependence on the laser intensity. In fact, transitions from higher rotational states over J = 60.5 of N_2O^+ in the $\tilde{X}\ ^2\Pi_{3/2}$ (000) state are observed by

increasing the intensity of the intense femtosecond laser pulses from 9.0×10^{13} W/cm^2 to 1.1×10^{14} W/cm^2. The obtained excitation spectra cannot be reproduced by the spectra calculated under the assumptions that rotational states of N_2O^+ in the $\tilde{X}\ ^2\Pi_{3/2}$ (000) state are thermally populated. A simplified model based on the polarizability interaction is built to reproduce the measured excitation spectra and to extract the rotational-state distribution of N_2O^+ in the $\tilde{X}\ ^2\Pi_{3/2}$ (000) state. In this model, N_2O molecules in the intense laser fields are rotationally excited by multiple Raman transitions induced by the polarizability interaction until the time $t = t_{switch}$, where t_{switch} is an adjustable parameter. After the ionization ($t_{switch} < t$), the rotational excitation processes of N_2O^+ in the $\tilde{X}\ ^2\Pi_{3/2}$ (000) state are induced in the intense laser fields. Excitation spectra calculated using this model agree well with the observed spectra. Therefore, it is concluded that the observed rotational excitation is attributed to the sequence of the rotational Raman excitation that occurs in the electronic and vibrational ground states of both N_2O molecules and N_2O^+ ions. The determined rotational-state distribution shows that high-J states are populated by the intense femtosecond laser pulses. The maximum values of J are about 53.5 and 61.5 when using the intense femtosecond laser pulses with intensities of 9.0×10^{13} W/cm^2 and 1.1×10^{14} W/cm^2, respectively. The higher rotational states are populated by stronger laser pulses because the polarizability interaction is enhanced as the laser intensity increases.

In addition to the rotational-state distribution, it is important to investigate whether the rotational states of N_2O^+ in the $\tilde{X}\ ^2\Pi_{3/2}$ (000) state are coherently populated. It is known that the rotational coherence of neutral molecules can be investigated using two intense femtosecond laser pulses. The populations of rotational states change with the delay between the two laser pulses if the rotational states of the molecules are coherently populated by the first laser pulse. In the present study, this experimental technique, which is well established for neutral molecules, is applied to molecular ions produced by the intense femtosecond laser pulses. Two intense femtosecond laser pulses are used to investigate how a change of the delay between the two intense laser pulses affects the rotational-state populations of the molecular ions generated by the first intense laser pulse. The nanosecond laser pulse mainly probes the population of $J = 40.5$. It is found that the population of this rotational state oscillates periodically by changing the delay between the two intense femtosecond laser pulses. This oscillation of the rotational-state

population is evidence that the several rotational states of N_2O^+ in the $\tilde{X}\ ^2\Pi_{3/2}$ (000) state are coherently populated. The similar oscillation of the rotational-state population is observed even when the population of the neighboring rotational state, J = 39.5, is monitored by the nanosecond laser pulse. The observed oscillations of the populations of J = 39.5 and 40.5 are in antiphase relation at delays of 1/8 τ_{rev} and 3/8 τ_{rev} even though both of the oscillatory signals are in phase each other at delays of 1/4 τ_{rev} and 1/2 τ_{rev}, where τ_{rev} is the revival time of $^2\Pi$ molecules (81.3 ps) and twice as large as the rotational period of $^1\Sigma^+$ molecules. It is shown that the antiphase behavior is attributed to the different dependence of the alignment dynamics on J.

Bibliography

[1] G. Magyar, Ultrashort laser pulses and their uses, Nature, **218**, 16 (1968)
[2] G. H. C. New, The generation of ultrashort laser pulses, Rep. Prog. Phys., **46**, 877 (1983)
[3] P. M. W. Fremch, The generation of ultrashort laser pulses, Rep. Prog. Phys., **58**, 169 (1995)
[4] T. Brabec and F. Krausz, Intense few-cycle laser fields: Frontiers of nonlinear optics, Rev. Mod. Phys. **72**, 545 (2000)
[5] U. Keller, Recent developments in compact ultrafast lasers, Nature, **424**, 831 (2003)
[6] T. H. Maiman, Stimulated optical radiation in ruby, Nature, **187**, 493 (1960)
[7] F. Rosca-Pruna and M. J. J. Vrakking, Experimental observation of revival structures in picosecond laser-induced alignment of I_2, Phys. Rev. Lett. **87**, 153902 (2001)
[8] T. S. Rose, M. J. Rosker, and A. H. Zeweil, Femtosecond real-time observation of wave packet oscillations (resonance) in dissociation reactions, J. Chem. Phys. **88**, 6672 (1988)
[9] P. B. Corkum and F. Krausz, Attosecond science, Nat. Phys. **3**, 381 (2007)
[10] M. F. Kling and M. J. J. Vrakking, Attosecond electron dynamics, Annu. Rev. Phys. Chem. **59**, 463 (2008)
[11] F. Krausz and M. Ivanov, Attosecond physics, Rev. Mod. Phys. **81**, 163 (2009)
[12] M. Uiberacker, Th. Uphues, M. Schultze, A. J. Verhoef, V. Yakovlev, M. F. Kling, J. Rauschenberger, N. M. Kabachnik, H. Schröder, M. Lezius, K. L. Kompa, H. -G. Muller, M. J. J. Vrakking, S. Hendel, U. Kleineberg, U. Heinzmann, M. Drescher, and F. Krausz, Attosecond real-time observation of electron tunneling in atoms, Nature, **446**, 627 (2007)
[13] E. Goulielmakis, Z. Loh, A. Wirth, R. Santra, N. Rohringer, V. S. Yakovlev, S. Zherebtsov, T. Pfeifer, A. M. Azzeer, M. F. Kling, S. Leone, and F. Krausz, Real-time observation of valence electron motion, Nature, **466**, 739 (2010)
[14] S. Backus, C. G. Durfee, III, M. M. Murnane, and H. C. Kapteyn, High power ultrafast lasers, Rev. Sci, Instrum. **69**, 1207 (1988)
[15] D. Strickland and G. Mourou, Compression of amplified chirped optical pulses, Opt. Commun. **55**, 447 (1985)
[16] G. A. Mourou, T. Tajima, S. V. Bulanov, Optics in the relativistic regime, Rev. Mod. Phys. **78**, 309 (2006)
[17] M. Protopapas, C. H. Keitel, and P. L. Knight, Atomic physics with super-high intensity lasers, Rep. Prog. Phys. **60**, 389 (1997)
[18] B. Sheehy and L. F. DiMauro, Atomic and molecular dynamics in intense optical fields, Annu. Rev. Phys. Chem. **47**, 463 (1996)
[19] K. Yamanouchi, The next frontier, Science, **295**, 1659 (2002)
[20] J. H. Posthumus, The dynamics of small molecules in intense laser fields, Rep. Prog. Phys. **67**, 623 (2004)
[21] A. Becker and F. H. M. Faisal, Intense-field many-body S-matrix theory, J. Phys. B: At. Mol. Opt. Phys. **38**, R1 (2005)
[22] P. Agostini and L. F. DiMauro, Atoms in high intensity mid-infrared pulses, Contemp. Phys. **49**, 179 (2008)

[23] C. Vozzi, M. Negro, and S. Stagira, Strong-field phenomena driven by mid-infrared ultrafast sources, J. Mod. Opt. **59**, 1283 (2012)
[24] L. F. DiMauro and P. Agostini, Ionization dynamics in strong laser fields, Adv. At. Mol. Phys. **35**, 79 (1995)
[25] N. B. Delone and V. P. Krainov, Tunneling and barrier-suppression ionization of atoms and ions in a laser radiation field, Physics-Uspekhi, **41**, 469 (1998)
[26] V. S. Popov, Tunnel and multiphoton ionization of atoms and ions in a strong laser field (Keldysh theory), Physics-Uspekhi, 47, **855** (2004)
[27] M. Y. Ivanov, M. Spanner, and O. Smirnova, Anatomy of strong field ionization, J. Mod. Opt. 52, 165 (2005)
[28] E. K. Damon and R. G. Tomlinson, Observation of ionization of gases by a ruby laser, Appl. Opt. 2, 546 (1963)
[29] A. L'Huillier, L. A. Lompré, G. Mainfray, and C. Manus, Multiply charged ions induced by multiphoton absorption processes in rare-gas atoms at 1.064 μm, J. Phys. B: At. Mol. Phys. **16**, 1363 (1983)
[30] P. Agostini, F. Fabre, G. Mainfray, and G. Petite, Free-free transitions following six-photon ionization of xenon atoms, Phys. Rev. Lett. **42**, 1127 (1979)
[31] G. Petite, P. Agostini, and H. G. Muller, Intensity dependence of non-perturbative above-threshold ionization spectra: experimental study, J. Phys. B: At. Mol. Opt. Phys. **21**, 4097 (1988)
[32] L. V. Keldysh, Ionization in the field of a strong electromagnetic wave, Sov. Phys. JETP, **20**, 1307 (1965)
[33] S. L. Chin, F. Yergeau, and P. Lavigne, Tunnel ionisation of Xe in an ultra-intense CO_2 laser field (10^{14} W cm^{-2}) with multiple charge creation, J. Phys. B: At. Mol. Phys. **18**, L213 (1985)
[34] P. F. Moulton, Spectroscopic and laser characteristics of Ti:Al_2O_3, J. Opt. Soc. Am. B, **3**, 125 (1986)
[35] T. Hatamoto, G. Prümper, M. Okunishi, D. Mathur, and K. Ueda, High-resolution electron-ion coincidence spectroscopy of ethanol in intense laser fields, Phys. Rev. A **75**, 061402(R) (2007)
[36] A. I. Nikishov and V. I. Ritus, Ionization of systems bound by short-range forces by the field of an electromagnetic wave, Sov. Phys. JETP, **23**, 162 (1966)
[37] A. M. Perelomov, V. S. Popov, and M. V. Terentev, Ionization of atoms in an alternating electric field, Sov. Phys. JETP, **23**, 924 (1966)
[38] A. M. Perelomov, V. S. Popov, and M. V. Terentev, Ionization of atoms in an alternating electric Field II, Sov. Phys. JETP, **24**, 207 (1967)
[39] A. M. Perelomov, and V. S. Popov, Ionization of atoms in an alternating electrical field III, Sov. Phys. JETP, **25**, 336 (1967)
[40] M. V. Ammosov, N. B. Delone, and V. P. Krainov, Tunnel ionization of complex atoms and atomic ions in an alternating electromagnetic field, Sov. Phys. JETP, **64**, 1191 (1986)
[41] L. Landau and E. M. Lifshitz, *Quantum Mechanics*, 3rd revised ed. (Pergamon, Oxford, 1977)
[42] W. Xiong and S. L. Chin, Tunnel ionization of potassium and xenon atoms in a high-intensity CO_2 laser radiation field, Sov. Phys. JETP, **72**, 268 (1991)

[43] S. Augst, D. D. Meyerhofer, D. Strickland, and S. L. Chin, Laser ionization of noble gases by Coulomb-barrier suppression, J. Opt. Soc. Am. B, **8**, 858 (1991)
[44] F. A. Ilkov, J. E. Decker, and S. L. Chin, Ionization of atoms in the tunneling regime with experimental evidence using Hg atoms, J. Phys. B: At. Mol. Opt. Phys, **25**, 4005 (1992)
[45] X. F. Li, A. L'Huillier, M. Ferray, L. A. Lompré, and G. Mainfray, Multiple-harmonic generation in rare gases at high laser intensity, Phys. Rev. A, 39, 5751 (1981)
[46] J. L. Krause, K. J. Schafer, and K. C. Kulander, High-order harmonic generation from atoms and ions in the high intensity regime, Phys. Rev. Lett. **68**, 3535 (1992)
[47] P. B. Corkum, Plasma perspective on strong-field multiphoton ionization, Phys. Rev. Lett. **71**, 1994 (1993)
[48] D. N. Fittinghoff, P. R. Bolton, B. Chang, and K. C. Kulander, Observation of nonsequential double ionization of helium with optical tunneling, Phys. Rev. Lett. **69**, 2642 (1992)
[49] B. Walker, B. Sheehy, L. F. DiMauro, P. Agostini, K. J. Schafer, and K. C. Kulander, Precision measurement of strong field double ionization of helium, Phys. Rev. Lett. **73**, 1227 (1994)
[50] D. N. Fittinghoff, P. R. Bolton, B. Chang, and K. C. Kulander, Polarization dependence of tunneling ionization of helium and neon by 120-fs pulses at 614 nm, Phys. Rev. A, 2174 (1994)
[51] C. Cornaggia, M. Schmidt, and D. Normand, Coulomb explosion of CO_2 in an intense femtosecond laser field, J. Phys. B: At. Mol. Opt. Phys. **27**, L123 (1994)
[52] C. Cornaggia, F. Salin, and C. Le Blanc, Changes in the SO_2 geometry during the laser-induced multiple ionization and fragmentation, J. Phys. B: At. Mol. Opt. Phys. **29**, L749 (1996)
[53] C. Cornaggia, Large-amplitude nuclear motions in the laser-induced Coulomb explosion of carbon dioxide molecules, Phys. Rev. A, **54**, R2555 (1996)
[54] A. Hishikawa, A. Iwamae, K. Hoshina, M. Kono, and K. Yamanouchi, Mass-resolved two-dimensional momentum imaging of the Coulomb explosion of N_2 and SO_2 in an intense laser field, Chem. Phys. Lett. **282**, 283 (1998)
[55] A. Hishikawa, A. Iwamae, K. Hoshina, M. Kono, and K. Yamanouchi, Coulomb-explosion dynamics of N_2O in intense laser-field: identification of new two-body and three-body fragmentation pathways, Res. Chem. Intermed. **24**, 765 (1998)
[56] A. Hishikawa, A. Iwamae, and K. Yamanouchi, Ultrafast deformation of the geometrical structure of CO_2 induced in intense laser fields, Phys. Rev. Lett. **83**, 1127 (1999)
[57] A. Hishikawa, A. Iwamae, and K. Yamanouchi, Ultrafast structural deformation of NO2 in intense laser fields studied by mass-resolved momentum imaging, J. Chem. Phys. **111**, 8871 (1999)
[58] J. H. Sanderson, A. El-Zein, W. A. Bryan, W. R. Newell, A. J. Langley, and P. F. Taday, Geometry modifications and alignment of H_2O in an intense femtosecond laser pulse, **59**, R2567 (1999)
[59] W. A. Bryan, J. H. Sanderson, A. El-Zein, W. R. Newell, P. F. Taday, and A. J. Langley, Laser-induced Coulomb explosion, geometry modification and reorientation of carbon dioxide, J. Phys. B: At. Mol. Opt. Phys. **33**, 745 (2000)
[60] H. Hasegawa, A. Hishikawa, and K. Yamanouchi, Coincidence imaging of Coulomb explosion of CS2 in intense laser fields, Chem. Phys. Lett. **349**, 57 (2001)
[61] A. Hishikawa, H. Hasegawa, and K. Yamanouchi, Sequential three-body Coulomb

explosion of CS_2 in intense laser fields appearing in momentum correlation map, Chem. Phys. Lett. **361**, 245 (2002)
[62] J. H. Sanderson, T. R. J. Goodworth, A. El-Zein, W. A. Bryan, W. R. Newell, A. J. Langley, and P. F. Taday, Coulombic and pre-Coulombic geometry evolution of carbonyl sulfide in an intense laser pulse, determined by momentum imaging, Phys. Rev. A **65**, 043403 (2002)
[63] K. Zhao, G. Zhang, and W. T. Hill III, Strong-field dissociative ionization of a linear triatomic molecule: Relationship between Coulomb-explosion energies and bond angle, Phys. Rev. A **68**, 063408 (2003)
[64] Y. Sato, H. Kono, S. Koseki, and Y. Fujimura, Description of molecular dynamics in intense laser fields by the time-dependent adiabatic state approach: application to simultaneous two-bond dissociation of CO_2 and its control, J. Am. Chem. Soc. **125**, 8019 (2003)
[65] A. Hishikawa, H. Hasegawa, and K. Yamanouchi, Nuclear dynamics on the light-dressed potential energy surface of CS_2 by coincidence momentum imaging, Chem. Phys. Lett. **388**, 1 (2004)
[66] H. Kono, Y. Sato, N. Tanaka, T. Kato, K. Nakai, S. Koseki, and Y. Fujimura, Quantum mechanical study of electronic and nuclear dynamics of molecules in intense laser fields, Chem. Phys. **304**, 203 (2004)
[67] A. Hishikawa, E. J. Takahashi, and A. Matsuda, Electronic and nuclear responses of fixed-in-space H_2S to ultrashort intense laser fields, Phys. Rev. Lett. **97**, 243002 (2006)
[68] J. P. Brichta, S. J. Walker, R. Helsten, and J. H. Sanderson, Ultrafast imaging of multielectronic dissociative ionization of CO_2 in an intense laser field, J. Phys. B: At. Mol. Opt. Phys. **40**, 117 (2007)
[69] A. Matsuda, E. J. Takahashi, and A. Hishikawa, Dalitz plot analysis of Coulomb exploding O_3 in ultrashort intense laser fields, J. Chem. Phys. 127, 114318 (2007)
[70] I. Bocharova, R. Karimi, E. F. Penka, J. P. Brichta, P. Lassonde, X. Fu, J. C. Kieffer, A. D. Bandrauk, I. Litvinyuk, J. Sanderson, and F. Légaré, Charge resonance enhanced ionization of CO_2 probed by laser Coulomb explosion imaging, Phys. Rev. Lett. **107**, 063201 (2011)
[71] A. Giusti-Suzor, F. H. Mies, L. F. DiMauro, E. Charron, and B. Yang, Dynamics of H_2^+ in intense laser fields, J. Phys. B: At. Mol. Opt. Phys. **28**, 309 (1995)
[72] B. Yang, L. Zhang, H. Xu, R. Li, and K. Yamanouchi, Fragmentation of hydrocarbon molecules in intense laser fields studied by coincidence momentum imaging: a review, Chin. J. Phys. **52**, 652 (2014)
[73] A. Talevpour, C. -Y. Chien, and S. L. Chin, The effects of dissociative recombination in multiphoton ionization of O_2, J. Phys. B: At. Mol. Opt. Phys., **29**, L677 (1996)
[74] C. Guo, M. Li, J. P. Nibarger, and G. N. Gibson, Single and double ionization of diatomic molecules in strong laser fields, Phys. Rev. A, **58**, 4271(R) (1998)
[75] E. Wells, M. J. DeWitt, and R. R. Jones, Comparison of intense-field ionization of diatomic molecules and rare-gas atoms, Phys. Rev. A **66**, 013409 (2002)
[76] Z. Y. Lin, X. Y. Jia, C. L. Wang, Z. Hu, H. P. Kang, W. Quan, X. Y. Lai, X. J. Liu, J. Chen, B. Zeng, W. Chu, J. P. Yao, Y. Cheng, and Z. Z. Xu, Ionization suppression of diatomic molecules in an intense midinfrared laser field, Phys. Rev. Lett. **108**, 223001 (2012)
[77] H. P. Kang, Z. Y. Lin, S. P. Xu, C. L. Wang, W. Quan, X. Y. Lai, and X. J. Liu, Wavelength-dependent ionization suppression of diatomic molecules in intense circularly polarized laser fields, Phys. Rev. A **90**, 063426 (2014)

[78] C. Guo, Multielectron effects on single-electron strong field ionization, Phys. Rev. Lett. **85**, 2276 (2000)
[79] J. Muth-Böhm, A. Becker, and F. H. M. Faisal, Suppressed molecular ionization for a class of diatomics in intense femtosecond laser fields, Phys. Rev. Lett. **85**, 2280 (2000)
[80] A. Saenz, On the influence of vibrational motion on strong-field ionization rates in molecules, J. Phys. B: At. Mol. Opt. Phys. **33**, 4365 (2000)
[81] X. M. Tong, Z. X. Zhao, and C. D. Lin, Theory of molecular tunneling ionization, Phys. Rev. A, **66**, 033402 (2002)
[82] B. K. McFarland, J. P. Farrell, P. H. Bucksbaum, and M. Gühr, High harmonic generation from multiple orbitals in N_2, Science **322**, 1232 (2008)
[83] H. Akagi, T. Otobe, A. Staudte, A. Shiner, F. Turner, R. Dörner, D. M. Villeneuve, and P. B. Corkum, Laser tunnel ionization from multiple orbitals in HCl, Science, **325**, 1364 (2009)
[84] O. Smirnova, Y. Mairesse, S. Patchkovskii, N. Dudovich, D. Villeneuve, P. Corkum, and M. Y. Ivanov, High harmonic interferometry of multi-electron dynamics in molecules, Nature, **460**, 972 (2009)
[85] C. Wu, H. Zhang, H. Yang, and Q. Gong, Tunneling ionization of carbon dioxide from lower-lying orbitals, Phys. Rev. A **83**, 033410 (2011)
[86] J. Wu, L. Ph. H. Schmidt, M. Kunitski, M. Meckel, S. Voss, H. Sann, H. Kim, T. Jahnke, A. Czasch, and R. Dörner, Multiorbital tunneling ionization of the CO molecule, Phys. Rev. Lett. **108**, 183001 (2012)
[87] J. Yao, G. Li, X. Jia, X. Hao, B. Zeng, C. Jing, W. Chu, J. Ni, H. Zhang, H. Xie, C. Zhang, Z. Zhao, J. Chen, X. Liu, Y. Cheng, and Z. Xu, Alignment-dependent fluorescence emission induced by tunneling ionization of carbon dioxide from lower-lying orbitals, Phys. Rev. Lett. **111**, 133001 (2013)
[88] M. Oppermann, S. J. Weber, F. Morales, M. Richter, S. Patchkovskii, A. Csehi, Á. Vibók, M. Ivanov, O. Smirnova, and J. P. Marangos, Control and identification of strong field dissociative channels in CO_2^+ via molecular alignment, J. Phys. B: At. Mol. Opt. Phys. **47**, 124025 (2014)
[89] J. Troβ, X. Ren, V. Makhija, S. Mondal, V. Kumarappan, and C. A. Trallero-Herrero, N_2 HOMO-1 orbital cross section revealed through high-order-harmonic generation, Phys. Rev. A **95**, 033419 (2017)
[90] H. Stapelfeldt and T. Seideman, Colloquium: Aligning molecules with strong laser pulses, Rev. Mod. Phys. **75**, 543 (2003)
[91] T. Seideman and E. Hamilton, Nonadiabatic alignment by intense pulses. Concepts, theory, and directions, Adv. At. Mol. Phys. **52**, 289 (2006)
[92] M. Lemeshko, R. V. Krems, J. M. Doyle, and S. Kais, Manipulation of molecules with electromagnetic fields, Mol. Phys. **111**, 1648 (2013)
[93] D. Pavičić, K. F. Lee, D. M. Rayner, P. B. Corkum, and D. M. Villeneuve, Direct measurement of the angular dependence of ionization for N_2, O_2, and CO_2 in intense laser fields, Phys. Rev. Lett. **98**, 243001 (2007)
[94] W. Fuβ, W. E. Schmid, and S. A. Trushin, Time-resolved dissociative intense-laser field ionization for probing dynamics: Femtosecond photochemical ring opening of 1,3-cyclohexadiene, J. Chem. Phys. **112**, 8347 (2000)

[95] S. Larimian, S. Erattupuzha, S. Mai, P. Marquetand, L. González, L. Baltuška, M. Kitzler, and X. Xie, Molecular oxygen observed by direct photoproduction from carbon dioxide, Phys. Rev. A **95**, 011404 (R) (2017)
[96] Th. Ergler, B. Feuerstein, A. Rudenko, K. Zrost, C. D. Schröter, R. Moshammer, and J. Ullrich, Quantum-phase resolved mapping of ground-state vibrational D_2 wave packets via selective depletion in intense laser pulses, Phys. Rev. Lett. **97**, 103004 (2006)
[97] Th. Ergler, A. Rudenko, B. Feuerstein, K. Zrost, C. D. Schröter, R. Moshammer, and J. Ullrich, Spatiotemporal imaging of ultrafast molecular motion: collapse and revival of the D_2^+ nuclear wave packet, Phys. Rev. Lett. **97**, 193001 (2006)
[98] H. Chen, V. Taglimonti, and G. N. Gibson, Internuclear separation dependent ionization of the valence orbitals of I_2 by strong laser fields, Phys. Rev. Lett. **109**, 193002 (2012)
[99] A. Matsuda, E. J. Takahashi, and A. Hishikawa, Time-resolved laser Coulomb explosion imaging using few-cycle intense laser pulses: Application to exploding CS_2 in highly charged states,
[100] S. Erattupuzha, S. Larimian, A. Baltuška, X. Xie, and M. Kitzler, Two-pulse control over double ionization pathways in CO_2, J. Chem. Phys. **144**, 024306 (2016)
[101] R. Forbes, A. E. Boguslavskiy, I. Wilkinson, J. G. Underwood, and A. Stolow, Excited state wavepacket dynamics in NO_2 probed by strong-field ionization, J. Chem. Phys. **147**, 054305 (2017)
[102] T. Endo, A. Matsuda, M. Fushitani, T. Yasuike, O. I. Tolstikhin, T. Morishita, and A. Hishikawa, Imaging Electronic Excitation of NO by Ultrafast Laser Tunneling Ionization, Phys. Rev. Lett. **116**, 163002 (2016)
[103] B. Ulrich, A. Vredenborg, A. Malakzadeh, L. Ph. H. Schmidt, T. Havermeier, M. Meckel, K. Cole, M. Smolarski, Z. Chang, T. Jahnke, and R. Dörner, Imaging of the structure of the argon and neon dimer, trimer, and tetramer, J. Phys. Chem. A **115**, 6936 (2011)
[104] J. Wu, M. Kunitski, L. Ph. H. Schmidt, T. Jahnke, and R. Dörner, Structures of N_2Ar, O_2Ar, and O_2Xe dimers studied by Coulomb explosion imaging, J. Chem. Phys. **137**, 104308 (2012)
[105] C. Figueira de Morisson Faira and X. Liu, Electron-electron correlation in strong laser fields, J. Mod. Opt, **58**, 1076 (2011)
[106] B. Fabre, J. H. Posthumus, L. Malfaire, E. M. Staicu-Casagrande, J. Jureta, C. Cornaggia, E. Baldit, and X. Urbain, First results on tunneling ionization of H_2 with a new portable experiment, Laser Physics, **14**, 468 (2004)
[107] X. Urbain, B. Fabre, E. M. Staicu-Casagrande, N. de Ruette, V. M. Andrianarijaona, J. Jureta, J. H. Posthumus, A. Saenz, E. Baldit, and C. Cornaggia, Intense-laser-field ionization of molecular hydrogen in the tunneling regime and its effect on the vibrational excitation of H_2^+, Phys. Rev. Lett. **92**, 163004 (2004)
[108] F. J. Lovas, Microwave spectral tables II. Triatomic molecules, J. Phys. Chem. Ref. Data, **7**, 1445 (1978)
[109] M. A. Gharaibeh and D. J. Clouthier, A laser-induced fluorescence study of the jet-cooled nitrous oxide cation (N_2O^+), J. Chem. Phys. **136**, 044318 (2012)
[110] R. Frey, R. Kakoschke, and E. W. Schlag, Spectroscopy of molecular ions: laser-induced fragmentation spectra of N_2O^+, $A\ ^2\Sigma^+$ - $X\ ^2\Pi$, Chem. Phys. Lett. **93**, 227 (1982)
[111] J. H. Callomon and F. Creutzberg, The electronic emission spectrum of ionized nitrous oxide, N_2O^+: $\widetilde{A}\ ^2\Sigma^+$ - $\widetilde{X}\ ^2\Pi$, Philos. Trans. R. Soc. London **277**, 157 (1974)
[112] J. T. Hougen, Rotational energy levels of a linear triatomic molecule in a $^2\Pi$ electronic

state, J. Chem. Phys. **36**, 519 (1962)
[113] C. E. Fellows, Improved molecular constants of the 000-000 band of the electronic transition of $A\,^2\Sigma^+$ - $X\,^2\Pi$ of N_2O^+ radical, J. Chem. Phys., **138**, 164316 (2013)
[114] R. S. Mulliken and A. Christy, *Λ*-type doubling and electron configurations in diatomic molecules, Phys. Rev., **38**, 87 (1931)
[115] G. Herzberg, *Molecular spectra and molecular structure I. Spectra of diatomic molecules* (D. Van Nostrand Co., New York, 1950)
[116] B. Friedrich and D. Herschbach, Alignment and trapping of molecules in intense laser pulses, Phys. Rev. Lett. **74**, 4623 (1995)
[117] H. Hasegawa and Y. Ohshima, Decoding the state distribution in a nonadiabatic rotational excitation by a nonresonant intense laser field, Phys. Rev. A, **74**, 061401 (R) (2006)
[118] J. Brown and A. Carrington, *Rotational spectroscopy of diatomic molecules* (Cambridge university press, 2003)
[119] R. N. Zare, *Angular momentum; Understanding spatial aspects in chemistry and physics* (Wiley-Internascience, 1988)
[120] P. M. Kraus, S. B. Zhang, A. Gijsbertsen, R. R. Lucchese, N. Rohringer, and H. J. Wörner, High-harmonic probing of electronic coherence in dynamically aligned molecules, Phys. Rev. Lett. **111**, 243005 (2013)
[121] S. B. Zhang, D. Baykusheva, P. M. Kraus, H. J. Wörner, and N. Rohringer, Theoretical study of molecular electronic and rotational coherences by high-order harmonic generation, Phys. Rev. A**, 91**, 023421 (2015)
[122] M.J.J. Vrakking and S. Stolte, Coherent control of molecular orientation, Chem. Phys. Lett. **271**, 209 (1997)
[123] T. Kanai and H. Sakai, Numerical simulations of molecular orientation using strong, nonresonant, two-color laser fields, J. Chem. Phys. **115**, 5492 (2001)
[124] R. W. Robinett, Quantum wave packet revivals, Phys. Rep. **392**, 1 (2004)
[125] J. Itatani, J. Levesque, D. Zeidler, H. Niikura, H, Pépin, J. C. Kieffer, P. B. Corkum, and D. M. Villeneuve, Tomographic imaging of molecular orbitals, Nature, **432**, 867 (2004)
[126] J. Itatani, D. Zeidler, J. Levesque, M. Spanner, D. M. Villeneuve, and P. B. Corkum, Controlling High Harmonic Generation with Molecular Wave Packet, Phys. Rev. Lett. **94**, 123902 (2005)
[127] T. Kanai, S. Minemoto, and H. Sakai, Quantum interference during high-order harmonic generation from aligned molecules, Nature, **435**, 470 (2005)
[128] R. M. Lock, X. Zhou, W. Li, M. M. Murnane, H. C. Kapteyn, Measuring the intensity and phase of high-order harmonic emission from aligned molecules, Chem. Phys. **336**, 22 (2009)
[129] R. M. Lock, S. Ramakrishna, X. Zhou, H. C. Kapteyn, M. M. Murnane, and T. Seideman, Extracting Continuum Electron Dynamics from High Harmonic Emission from Molecules, Phys. Rev. Lett. **108**, 133901 (2012)
[130] X. Ren, V. Makhija, A. -T. Le, J. Troβ, S. Mondal, C. Jin, V. Kumarappan, and C. Trellero-Herrero, Measuring the angle-dependent photoionization cross section of nitrogen using high-harmonic generation, Phys. Rev. A **88**, 043421 (2013)
[131] I. V. Litvinyuk, K. F. Lee, P. W. Dooley, D. M. Rayber, D. M. Villeneuve, and P. B. Corkum, Alignment-dependent strong field ionization of molecules, Phys. Rev. Lett. 90, 233003 (2003)
[132] Z. X. Zhao, X. M. Tong, and C. D. Lin, Alignment-dependent ionization probability of

molecules in a double-pulse laser field, Phys. Rev. A **67**, 043404 (2003)
[133] X. Xie, K. Doblhoff-Dier, H. Xu, S. Roither, M. S. Schöffler, D. Kartashov, S. Erattupuzha, T. Rathje, G. G. Paulus, K. Yamanouchi, A. Baltuška, S. Gräfe, and M. Kitzler, Selective control over fragmentation reactions in polyatomic molecules using impulsive laser alignment, Phys. Rev. Lett. **112**, 163003 (2014)
[134] C. Cornaggia, Temporal analysis of fractional revivals of molecular observables following impulsive alignment, Phys. Rev. A **91**, 043426 (2015)
[135] H. Hasegawa, Y. Ikeda, K, Sonoda, T. Sato, A. Iwasaki, and K. Yamanouchi, Angular dependence of ionization probability of C_2H_2 in a linearly polarized intense laser field, Chem. Phys. Lett. **662**, 235 (2016)
[136] S. Ramakrishna and T. Seideman, Information content of high harmonics generated from aligned molecules, Phys. Rev. Lett. **99**, 113901 (2007)
[137] S. Ramakrishna and T. Seideman, High-order harmonic generation as a probe of rotational dynamics, Phys. Rev. A, **77**, 053411 (2008)
[138] J. L. Hansen, L. Holmegaard, J. H. Nielsen, H. Stapelfeldt, D. Dimitrovski, and L. B. Madsen, Orientation-dependent ionization yields from strong field ionization of fixed-in-space linear and asymmetric top molecules, J. Phys. B: At. Mol. Opt. Phys. **45**, 015101 (2012)
[139] D. Dimitrovski, M. Abu-samha, L. B. Madsen, F. Filsinger, G. Meijer, J. Küpper, L. Holmegaard, L. Kalhøj, J. H. Nielsen, and H. Stapelfeldt, Ionization of oriented carbonyl sulfide molecules by intense circularly polarized laser pulses, Phys. Rev. A **83**, 023405 (2011)
[140] D. Dimitrovski, J. Maurer, H. Stapelfeldt, and L. B. Madsen, Strong-field ionization of three-dimensionally aligned naphthalene molecules: orbital modification and imprints of orbital nodal planes, J. Phys. B: At. Mol. Opt. Phys. **48**, 245601 (2015)
[141] R. Johansen, K. G. Bay, L. Christensen, J. Thøgersen, D. Dimitrovski, L. B. Madsen, and H. Stapelfeldt, Alignment-dependent strong-field ionization yields of carbonyl sulfide molecules induced by mid-infrared laser pulses, J. Phys. B: At. Mol. Opt. Phys. **49**, 205601 (2016)
[142] X. M. Tong and C. D. Lin, Emprical formula for static field ionization rates of atoms and molecules by lasers in the barrier-suppression regime, J. Phys. B: At. Mol. Opt. Phys. **38**, 2593 (2005)
[143] K. Doblhoff-Dier, M. Kitzler, and S. Gräfe, Theoretical investigation of alignment-dependent intense-field fragmentation of acetylene, Phys. Rev. A **94**, 013405 (2016)
[144] W. C. Wiley and I. H. McLaren, Time-of-flight mass spectrometer with improved resolution, Rev. Sci. Instrum. **26**, 1150 (1955)
[145] J. E. Sansonetti, and W. C. Martin, Handbook of basic atomic spectroscopic data, J. Phys. Chem. Ref. Data, **34**, 1559 (2005)
[146] A. S. Newton, Triple ionization in small molecules, J. Chem. Phys. **40**, 607 (1964)
[147] J. H. D. Eland, M. Hochlaf, P. Linusson, E. Anderson, L.Hedin, and R. Feifel, Triple ionization spectra by coincidence measurements of double Auger decay: The case of OCS, J. Chem. Phys. **132**, 014311 (2010)
[148] W. A. Bryan, W. R. Newell, J. H. Sanderson, A. J. Langley, Observation of multiple ionization pathways for OCS in an intense laser field resolved by three-dimensional covariance mapping and visualized by hierarchical ionization topology, Phys. Rev. A **74**, 053409 (2006)
[149] S. Stimson, M. Evans, C. Y. Ng, C. –W. Hsu, P. Heimann, C. Destandau, G. Chambaud, and P. Rosmus, High resolution vasuum ultraviolet pulsed field ionization photoelectron band for OCS^+ ($X^2\Pi$): An experimental and theoretical study, J. Chem. Phys. **108**, 6205 (1998)

[150] R. Weinkauf and U. Boesl, Laser spectroscopy of molecular ions: The A-X transition in the OCS radical cation, J. Chem. Phys. **101**, 8482 (1994)
[151] G. Maroulis and M. Menadakis, Polarizability and hyperpolarizability of COS and NNO, Chem. Phys. Lett. **494**, 144 (2010)
[152] H. Ohmura, N. Saito, and T. Morishita, Molecular tunneling ionization of the carbonyl sulfide molecule by double-frequency phase-controlled laser fields, Phys. Rev. A **89**, 013405 (2014)
[153] A. Abdurrouf and F. H. M. Faisal, Theory of intense-field dynamic alignment and high-order harmonic generation from coherently rotating molecules and interpretation of intense-field ultrafast pump-probe experiments, Phys. Rev. A **79**, 023405 (2009)
[154] L. S. Wang, J. E. Reutt, Y. T. Lee, and D. A. Shirley, High resolution UV photoelectron spectroscopy of CO_2^+, COS^+, and CS_2^+ using supersonic molecular beams, J. Electron Spectrosc. Relat. Phenom. **47**, 167 (1988)
[155] V. Brites, J. H. D. Eland, M. Hochlaf, OCS^{2+} dication spectroscopy and electronic states, Chemical Physics, **346**, 23 (2008)
[156] R. I. Hall, L. Avaldi, G. Dawber, A. G. McConkey, M. A. MacDonald, G. C. King, Double photoionization of CO_2, OCS, C_2H_2, CF_4 and C_6H_6 studied by threshold photoelectrons coincidence (TPEsCO) spectroscopy, Chem. Phys. **187**, 125 (1994)
[157] C. Cornaggia and Ph. Hering, Nonsequential double ionization of small molecules induced by a femtosecond laser field, Phys. Rev. A **62**, 023403 (2000)
[158] X. Liu, C. Wu, Z. Wu, Y. Liu, Y. Deng, and Q. Gong, Recollision-induced dissociation and ionization of oxygen in few-cycle laser fields, Phys. Rev. A **83**, 035403 (2011)
[159] P. W. Dooley, I. V. Litvinyuk, K. F. Lee, D. M. Rayner, M. Spanner, D. M. Villeneuve, and P. B. Corkum, Direct imaging of rotational wave-packet dynamics of diatomic molecules, Phys. Rev. A **68**, 023406 (2003)
[160] H. J. Wörner and P. B. Corkum, Imaging and controlling dynamics by laser-induced tunnel ionization, J. Phys. B: At. Mol. Opt. Phys. **44**, 041001 (2011)
[161] P. M. Kraus, B. Mignolet, D. Baykusheva, A. Rupenyan, L. Horný, E. F. Penka, G. Grassi, O. I. Tolstikhin, J. Schneider, F. Jensen, L. B. Madsen, A. D. Bandrauk, F. Remacke, H. J. Wörner, Measurement and laser control of attosecond charge migration in ionized iodoacetylene, Science, **350** 6262 (2015)
[162] L. Fechner, N. Camus, J. Ullrich, T. Pfeifer, and R. Moshammer, Strong-field tunneling from a coherent superposition of electronic states, Phys. Rev. Lett. **112**, 213001 (2014)
[163] J. Breidbach and L. S. Cederbaum, Migration of holes: Formalism, mechanisms, and illustrative applications, J. Chem. Phys. **118**, 3983 (2003)
[164] S. De, I. Znakovskaya, D. Ray, F. Anis, N. G. Johnson, I. A. Bocharova, M. Magrakvelidze, B. D. Esry, C. L. Cocke, I. V. Litvinyuk, and M. F. Kling, Field-free orientation of CO molecules by femtosecond two-color laser fields, Phys. Rev. Lett. **103**, 153002 (2009)
[165] S. Fleischer, Y. Zhou, R. W. Field, and K. A. Nelson, Molecular orientation and alignment by intense single-cycle THz pulses, Phys. Rev. Lett. **107**, 163603 (2011)
[166] P. M. Kraus, A. Rupenyan, and H. J. Wörner, High-harmonic spectroscopy of oriented OCS molecules: Emission of even and odd harmonics, Phys. Rev. Lett. **109**, 233903 (2012)
[167] E. Frumker, C. T. Hebeisen, N. Kahumba, J. B. Bertrand, H. J. Wörner, M. Spanner, D. M. Villeneuve, A. Naumov, and P. B. Corkum, Oriented rotational wave-packet dynamics studies via high harmonic generation, Phys. Rev. Lett. **109**, 113901 (2012)

[168] K. Kitano, N. Ishii, N. Kanda, Y. Matsumoto, T. Kanai, M. Kuwata-Gonokami, and J. Itatani, Orientation of jet-cooled polar molecules with an intense single-cycle THz pulse, Phys. Rev. A **88**, 061405(R) (2013)
[169] I. Znakovskaya, M. Spanner, S. De, H. Li, D. Ray, P. Corkum, I. V. Litvinyuk, C. L. Cocke, and M. F. Kling, Transition beteween mechanisms of laser-induced field-free molecular orientation, Phys. Rev. Lett. **112**, 113005 (2014)
[170] K. N. Egodapitiya, S. Li, and R. R. Jones, Terahertz-induced field-free orientation of rotationally excited molecules, Phys. Rev. Lett. **112**, 103002 (2014)
[171] K. Kitano, N. Ishii, T. Kanai, and J. Itatani, Selecting rotational two-level coherence in polar molecules by double terahertz pulses, Phys. Rev. A **90**, 041402(R) (2014)
[172] M. Spanner, S. Patchkovskii, E. Frumker, and P. Corkum, Mechanisms of two-color laser-induced field-free molecular orientation, Phys. Rev. Lett. **109**, 113001 (2012)
[173] P. M. Kraus, O. I. Tolstikhin, D. Baykusheva, A. Rupenyan, J. Schneider, C. Z. Bisgaard, T. Morishita, F. Jensen, L. B. Madsen, and H. J. Wörner, Observation of laser-induced electronic structure in oriented polyatomic molecules, Nat. Commun. **6** 7039 (2015)
[174] X. Ren, V. Makhija, H. Li, M. F. Kling, and V. Kumarappan, Alignment-assisted field-free orientation of rotationally cold CO molecules, Phys. Rev. A **90**, 013419 (2014)
[175] S. Zhang, C. Lu, T. Jia, Z. Wang, and Z. Sun, Controlling field-free molecular orientation with combined single- and dual-color laser pulses, Phys. Rev. A, **83**, 043410 (2011)
[176] R. Tehini, M. Z. Hoque, O. Faucher, and D. Sugny, Field-free molecular orientation of $^1\Sigma$ and $^2\Pi$ molecules at high temperature, Phys. Rev. A **85**, 043423 (2012)
[177] K. Nakajima, H. Abe, and Y. Ohtsuki, Optimal control simulation of field-free molecular orientation: alignment-enhanced molecular orientation, J. Phys. Chem. A, **116**, 11219 (2012)
[178] P. M. Kraus, D. Baykusheva, and H. J. Wörner, Two-pulse orientation dynamics and high-harmonic spectroscopy of strongly oriented molecules, J. Phys. B: At. Mol. Opt. Phys. **47**, 124030 (2014)
[179] P. M. Kraus, D. Baykusheva, and H. J. Wörner, Two-pulse field-free orientation reveals anisotropy of molecular shape resonance, Phys. Rev. Lett. **113**, 023001 (2014)
[180] K. Sonoda, A. Iwasaki, K. Yamanouchi, and H. Hasegawa, Enhancement of field-free molecular orientation of OCS by intense laser fields, AIP Conference Proceedings, **1906**, 030026 (2017)
[181] A. Goban, S. Minemoto, and H.Sakai, Laser-field-free molecular orientation, Phys. Rev. Lett. **101**, 013001 (2008)
[182] M. E. Sukharev and V. P. Krainov, Franck-Condon factors for the ionization of hydrogen and deuterium molecules in laser fields, JETP, **83**, 457 (1996)
[183] M. E. Sukharev and V. P. Krainov, Field-dependent Franck-Condon factors for the ionization of molecular hydrogen and deuterium, Laser Physics, **7**, 323 (1997)
[184] H. Zhang, C. Jing, J. Yao, G. Li, B. Zeng, W. Chu, J. Ni, H. Xie, H. Xu, S. L. Chin, K. Yamanouchi, Y. Cheng, and Z. Xu, Rotational coherence encoded in an "air-laser" spectrum of nitrogen molecular ions in an intense laser field, Phys. Rev. X, **3**, 041009 (2013)
[185] B. Zeng, W. Chu, G. Li, J. Yao, H. Zhang, J. Ni, C. Jing, H. Xie, and Y. Cheng, Real-time observation of dynamics in rotational molecular wave packets by use of air-laser spectroscopy, Phys. Rev. A **89**, 042508 (2014)
[186] H. Xie, B. Zeng, G. Li, W. Chu, H. Zhang, C. Jing, J. Yao, J. Ni, Z. Wang, Z. Li, and Y. Cheng, Coupling of N_2^+ rotational states in an air laser from tunnel-ionized nitrogen molecules,

Phys. Rev. A **90**, 042504 (2014)
[187] H. Salami and A. J. Ross, A molecular iodine atlas in ascii format, J. Mol. Spectrosc. **233**, 157 (2005)
[188] J. A. Beswick and M. Horani, Electronic predissociation in N_2O^+ model calculations for the $\tilde{A}\ ^2\Sigma^+$ state, Chem. Phys. Lett. **78**, 4 (1981)
[189] G. Chambaud, H. Gritli, P. Rosmus, H. -J. Werner, and P. J. Knowles, The ion-molecule reaction O^+ (^4S) + $N_2(X\ ^1\Sigma^+) \rightarrow NO^+(X^1\Sigma^+)$ + $N(^4S)$ and the predissociation of the A $^2\Sigma^+$ and B $^2\Pi$ states of N_2O^+, Mol. Phys. **98**, 1793 (2000)
[190] S. D. Price, J. H. D. Eland, P. G. Fournier, J. Fournier, and P. Millie, Electronic states and decay mechanisms of the N_2O^{2+} dication, J. Chem. Phys. **88**, 1511 (1988)
[191] T. A. Field and J. H. D. Eland, Lifetimes of metastable molecular doubly charged ions, Chem. Phys. Lett. **221**, 436 (1993)
[192] J. H. D. Eland, Complete double photoionization spectra of small molecules from TOF-PRPRCO measurements, Chem. Phys. 294, 171 (2003)
[193] S. Taylor, J. H. D. Eland, and M. Hochlaf, Fluorescence and metastability of N_2O^{2+}: Theory and experiment, J. Chem. Phys. **124**, 204319 (2006)
[194] E. Kinmond, J. H. D. Eland, and L. Karlsson, Dissociation of N_2O^+ ions from the valence states reached by one-photon photoionisation, Int. J. Mass Spectrom. **185/186/187**, 437 (1999)
[195] D. Klapstein and J. P. Maier, Lifetimes of N_2O^+ ($\tilde{A}\ ^2\Sigma^+$) and COS^+ ($\tilde{A}\ ^2\Pi$) in selected vibronic levels, Chem. Phys. Lett. **83**, 590 (1981)
[196] C. R. Brundle and D. W. Turner, Studies on the photoionisation of the linear triatomic molecules: N_2O, OCS, CS_2 and CO_2 using high-resolution photoelectron spectroscopy, Int. J. Mass. Spectrom., **2**, 195 (1969)
[197] S. Abed, M. Broyer, M. Carré, M. L. Gaillard, and M. Larzilliere, High-resolution spectroscopy of N_2O^+ in the near ultraviolet using FIBLAS (Fast-Ion-Beam Laser Spectroscopy), Chem. Phys. **74**, 97 (1983)
[198] J. Lerme, S. Abed, R. A. Holt, M. Larzilliere, and M. Carre, Measurement of the fragment kinetic energy distribution in laser photopredissociation of N_2O^+, Chem. Phys. Lett. **96**, 403 (1983)
[199] J. Lermé, S. Abed, M. Larzillière, R. A. Holt, and M. Carré, Kinetic energy spectrum of NO^+ photofragments from the photopredissociation of the $\tilde{A}\ ^2\Sigma^+$ state of N_2O^+, J. Chem. Phys. **84**, 2167 (1986)
[200] M. Larzillière, K. Gragued, and J. Lerme, *l*-type resonance and *l*-uncoupling in N_2O^+: observation of A $^2\Sigma^+$ - $^2\Phi$ transition, Chem. Phys. Lett. **134**, 467 (1987)
[201] H. Xu, Y. Guo, Q. Li, S. Liu, X. Ma, J. Liang, and H. Li, Spectroscopic study of N_2O^+ (*A* $^2\Sigma^+$) by photofragment excitation spectrum, J. Chem. Phys. **119**, 11609 (2003)
[202] H. Xu, Y. Guo, Q. Li, Y. Shi, S. Liu, and X. Ma, Channel switching effect in photodissociating N_2O^+ ion at 312.5 nm, J. Chem. Phys., **121**, 3069 (2004)
[203] H. Wang, X. Zhou, S. Liu, B. Jiang, D. Dongxu, and X. Yang, Predissociation dynamics of N_2O^+ at the *A* $^2\Sigma^+$ state: Three pathways to form NO^+ ($^1\Sigma^+$) revealed from ion velocity imaging, J. Chem. Phys., **132**, 244309 (2010)
[204] M. Ueyama, H. Hasegawa, A. Hishikawa, and K. Yamanouchi, Concerted and sequential Coulomb explosion processes of N_2O in intense laser fields by coincidence momentum imaging, J. Chem. Phys. **123**, 154305 (2005)
[205] J. P. Brichta, W. -K. Liu, A. A. Zaidi, A. Trottier, and J. H. Sanderson, Comparison of

ADK ionization rates as a diagnostic for selective vibrational level population measurement, J. Phys. B: At. Mol. Opt. Phys. **39**, 3769 (2006)
[206] J. L. Griggs Jr. and K. N. Rao, Vibration rotation bands of $^{15}N_2{}^{18}O$ determination of precise values of internuclear distances, J. Mol. Spectrosc. **25**, 34 (1968)
[207] H. M. Rosenstock, Harmonic oscillator Franck-Condon factors for the ionization of N_2O, Int. J. Mass. Spectrom. Ion Phys., **7**, 33 (1971)
[208] T. K. Kjeldsen and L. B. Madsen, Vibrational excitation of diatomic molecular ions in strong field ionization of diatomic molecules, Phys. Rev. Lett. **95**, 073004 (2005)
[209] A. Fleischer, H. J. Wörner, L. Arissian, L. R. Liu, M. Meckel, A. Rippert, R. Dörner, D. M. Villeneuve, P. B. Corkum, and A. Staudte, Probing angular correlations in sequential double ionization, Phys. Rev. Lett. **107**, 113003 (2011)
[210] L. Fechner, N. Camus, J. Ullrich, T. Pfeifer, and R. Moshammer, Strong-field tunneling from a coherent superposition of electronic states, Phys. Rev. Lett. **112**, 213001 (2014)
[211] Z.-H. Loh, M. Khalil, R. E. Correa, R. Santra, C. Buth, and S. R. Leone, Quantum state-resolved probing of strong-field-ionized xenon atoms using femtosecond high-order harmonic transient absorption spectroscopy, Phys. Rev. Lett. **98**, 143601 (2007)
[212] M. W. Schmidt, K. K. Baldridge, J. A. Boatz, S. T. Elbert, M. S. Gordon, J. H. Jensen, S. Koseki, N. Matsunaga, K. A. Nguyen, S. Su, T. L. Windus, M. Dupuis, J. A. Montgomery, General atomic and molecular electronic structure system, J. Comput. Chem. **14**, 1347 (1993)
[213] H. Kling and W. Hüttner, the temperature dependence of the Cotton-Mouton effect of N_2, CO, N2O, CO_2, OCS, and CS_2 in the gaseous state, Chem. Phys. **90**, 207 (1984)
[214] G. R. Alms, A. K. Burnham, and W. H. Flygare, Measurement of the dispersion in polarizability anisotropies, J. Chem. Phys. **63**, 3321 (1975)
[215] Y. Morioka, S. Hara, and M. Nakamura, Rotational intensity distribution in the H_2 photoelectron spectrum, Phys. Rev. A, **22**, 177 (1980)
[216] J. E. Pollard, D. J. Trevor, J. E. Reutt, Y. T. Lee, and D. A. Shirley, Rotationally resolved photoelectron spectroscopy of *n*-H_2, *p*-H_2, HD, and D_2, J. Chem. Phys. **77**, 34 (1982)
[217] S. T. Pratt, P. M. Dehmer, and J. L. Dehmer, Resonant multiphoton ionization of H_2 via the B $^1\Sigma_u^+$, v = 7, J = 2 and 4 levels with photoelectron energy analysis, J. Chem. Phys. **78**, 4315 (1983)
[218] W. G. Wilson, K. S. Viswanathan, E. Sekreta, and J. P. Reilly, Rotationally resolved laser photoelectron spectrum of gas-phase NO, J. Phys. Chem., **88**, 672, (1984)
[219] K. Müller-Dethlefs, M. Sander, and E. W. Schlag, Two-colour photoionization resonance spectroscopy of NO: Complete separation of rotational levels of NO^+ at the ionization threshold, Chem. Phys. Lett. 112, 291 (1984)
[220] S. N. Dixit and V. McKoy, Ionic rotational selection rules for (n + 1) resonant enhanced multiphoton ionization, Chem. Phys. Lett., **128**, 49 (1986)
[221] M. Sander, L. A. Cherter, K. Müller-Dethlefs, and E. W. Schlag, High-resolution zero-kinetic-energy photoelectron spectroscopy of nitric oxide, Phys. Rev. A, **36**, 4543 (1987)
[222] T. Trickl, E. F. Cromwell, Y. T. Lee, and A. H. Kung, State-selective ionization of nitrogen in the X $^1\Sigma_u^+$ v_+ = 0 and v_+ = 1 states by two-color (1+1) photon excitation near threshold, J. Chem. Phys., **91**, 6006 (1989)
[223] H. Ohmura, T. Nakanaga, and M. Tachiya, Coherent control of photofragment separation in the dissociative ionization of IBr, Phys. Rev. Lett. **92**, 113002 (2004)
[224] J. Wang, S. Zhao, C. Zhang, W. Li, and X. Zhou, Determination of structure parameters in

molecular tunneling ionisation model, Mol. Phys. **112**, 1102 (2014)
[225] Th. Ergler, A. Rudenko, B. Feuerstein, K. Zrost, C. D. Shröter, R. Moshammer, and J. Ullrich, Spatiotemporal imaging of ultrafast molecular motion: collapse and revival of the D_2^+ nuclear wave packet, Phys. Rev. Lett. **97**, 193001 (2006)
[226] I. A. Bocharova, H. Machiko, M. Magrakvelidze, D. Ray, P. Ranitovic, C. L. Cocke, and I. V. Litvinyuk, Direct Coulomb-explosion imaging of coherent nuclear dynamics induced by few-cycle laser pulses in light and heavy hydrogen, Phys. Rev. A **77**, 053407 (2008)
[227] A. S. Meijer, Y. Zhang, D. H. Parker, W. J. van der Zande, A. Gijsbertsen, and M. J. J. Vrakking, Controlling rotational state distributions using two-pulse stimulated Raman excitation, Phys. Rev. A **76**, 023411 (2007)
[228] Y. Ohshima and H. Hasegawa, Coherent rotational excitation by intense nonresonant laser fields, Int. Rev. Phys. Chem., 29, 619 (2010)
[229] A. Rouzée, A. Gijsberstsen, O. Ghafur, O. M. Shir, T. Bäck, S. Stolte, and M. J. J. Vrakking, Optimization of laser field-free orientation of a state-selected NO molecular sample, New J. Phys. **11**, 105040 (2009)